Inhibition of Pancreatic Stellate Cell Activation by Halofuginone Prevents Pancreatic Xenograft Tumor Development

Itai Spector, MSc,† Hen Honig, DVM,* Norifumi Kawada, MD,‡ Arnon Nagler, MD,§ Olga Genin, MSc,* and Mark Pines, PhD**

Objectives: Most solid tumors consist of neoplastic and nonneoplastic cells and extracellular matrix components. In the pancreas, activated stellate cells (PSCs) are the source of the extracellular matrix proteins. We evaluated the significance of PSC activation in tumor establishment and development in mouse xenografts.

Methods: Xenografts were established by implanting human pancreatic cancer cells (MiaPaca-2) subcutaneously or orthotopically by injecting them into the spleen. Fibrosis was induced by cerulein. Collagen level was evaluated by Sirius red staining. Prolyl 4-hydroxylase β and stellate cell activation–associated protein (Cygb/STAP) were determined by immunohistochemistry.

Results: Halofuginone inhibited subcutaneous tumor development implanted with Matrigel and reduced collagen and prolyl 4-hydroxylase β levels. Few tumors, which developed slowly, were observed after MiaPaca-2 implantation without Matrigel. Increase in tumor number and rate of development were observed with addition of PSCs from control pancreas, and further increase was observed when the PSCs were from cerulein-treated mice. Preincubation of the PSCs with halofuginone elicited Cygb/STAP level reduction and tumor growth inhibition. More tumors developed orthotopically in cerulein-treated mice than in controls; this was prevented by halofuginone.

Conclusions: Extracellular matrix production by activated PSCs is essential for tumor establishment and growth. Thus, inhibition of PSC activation is a viable means of reducing pancreatic tumor development.

Key Words: collagen, cytoglobin, halofuginone, fibrosis, xenograft

(*Pancreas* 2010;39: 1008–1015)

Most solid tumors consist of a mixture of neoplastic and nonneoplastic cells, together with extracellular matrix (ECM) components. This cellular microenvironment directly modulates tissue architecture, cell morphology, and cell fate,[1] and the ECM–stromal cell interaction contributes to the neoplastic phenotype.[2,3] Conversion of fibroblasts into myofibroblasts, mediated by transforming growth factor β (TGF-β) is the most prominent stromal reaction in many epithelial lesions.[4–7] The myofibroblasts are associated with the tumor cells at all stages of cancer progression,[8] and in various malignancies, tumor-dependent differentiation of fibroblasts toward myofibroblasts promotes further neoplastic progression.[9–12] The myofibroblasts synthesize large amounts of ECM components, especially collagen type I, which promotes tumor cell survival, reduces apoptosis, and serves as a signal for tumor cell invasion.[13–16] In the pancreas, the pancreatic stellate cells (PSCs) constitute the major source of the ECM proteins.[17–19] These cells are usually quiescent, with a low proliferation rate; however, upon activation, probably because of injury, they differentiate into myofibroblast-like cells, proliferate, and migrate to sites of tissue damage, where they synthesize ECM components to promote tissue repair.[20] These activated PSCs play a major role in the growth and development of pancreas adenocarcinoma, [20–25] and the tumor cells, in turn, stimulate PSC motility and attract them toward the tumor.[26] Similarly to chronic pancreatitis, adenocarcinoma of the pancreas has a remarkable fibrotic component,[27] and most examples exhibited fibroblast markers that were significantly more pronounced in tumor-associated myofibroblasts immediately adjacent to the tumor than in surrounding ones.[28] The TGF-β pathway is one of the signaling systems that has been identified as a major contributor to pancreatic cancer,[29] and a hallmark of pancreatic ductal adenocarcinoma is the presence of desmoplasia, which is defined as proliferation of fibrotic tissue with altered ECM, conducive to tumor growth and metastasis.[30] The desmoplasia is created by activated PSCs, which are stimulated by the cancer cells and thereby influence tumor aggressiveness.[21] In liver and pancreas, the stellate cell activation–association protein, also known as cytoglobin (Cygb/STAP) is a gene associated with collagen synthesis that is upregulated in activated stellate cells by TGF-β.[31] Although its specific role is yet to be elucidated, a potential role in the detoxification of reactive oxygen species in tumors and other pathological findings was suggested.[32,33]

Previously, we demonstrated that halofuginone, an analog of the plant alkaloid febrifugine, can inhibit hepatic and PSC activation[34–36] and the fibroblast-to-myofibroblast transition in the tumor microenvironment.[7,37] Halofuginone inhibited Smad3 phosphorylation downstream of the TGF-β signaling pathway,[38–41] resulting in reduction in collagen synthesis and fibrosis of various organs[42–44] and in tumors of diverse origins.[37,45–47] In the present study, we evaluated the effect of halofuginone-dependent inhibition of PSC activation on pancreatic tumor establishment and development, in subcutaneous and orthotopic xenografts mouse models.

MATERIALS AND METHODS

Materials

Fetal calf serum, Dulbecco's modified Eagle medium, and trypsin-EDTA solution (0.02%–0.25%) were obtained from Biochemical Industries (Bet Haemek, Israel). Cerulein and collagenase IV were obtained from Sigma (St Louis, Mo), and Sirius red F3B from BDH Laboratory Supplies (Poole, England).

From the *Institute of Animal Sciences, the Volcani Center, Bet Dagan, Israel; †Department of Animal Science, Faculty of Agriculture, The Hebrew University of Jerusalem, Israel; ‡Department of Hepatology, Graduate School of Medicine, Osaka City University, Japan; and §Department of Hematology and Bone Marrow Transplantation, Chaim Sheba Medical Center, Tel Hashomer, Israel.

Received for publication September 23, 2009; accepted February 12, 2010.

Reprints: Mark Pines, PhD, Institute of Animal Sciences, ARO, the Volcani Center, Bet Dagan 50250, Israel (e-mail: pines@agri.huji.ac.il).

This article is a contribution from the ARO, the Volcani Center, Bet Dagan, Israel.

Matrigel, a basement membrane preparation extracted from the Engelbreth-Holm-Swarm mouse sarcoma, a tumor rich in ECM proteins, was obtained from Becton Dickinson (Bedford, Mass). Halofuginone bromhydrate was obtained from Collgard Biopharmaceuticals Ltd (Tel Aviv, Israel). Antibodies to Cygb/STAP were prepared as previously described,[31] and prolyl 4-hydroxylase β (P4Hβ) monoclonal antibodies were from Acris (Hiddenhausen, Germany). The proliferating cell nuclear antigen staining kit was from Zymed Laboratories, Inc (South San Francisco, Calif).

Cell Culture

Pancreatic stellate cells were prepared either from naive mice or from mice treated with a single injection of cerulein (50 μg/kg).[36,48] After 24 hours, the pancreas was excised, freed from fat and lymph nodes, and digested with collagenase IV (0.02%), and the resulting suspension of cells was centrifuged at 1200*g* for 5 minutes. The cells were washed and resuspended in Dulbecco's modified Eagle medium containing 10% fetal bovine serum and antibiotics (penicillin, 100 U/mL; streptomycin, 100 mg/mL) and plated on 6-well plates with the same medium. All cells were incubated at 37°C in a humidified atmosphere containing 5% CO_2. Before implantation, cells were incubated with 25 nM halofuginone for 48 hours.

Animals and Experimental Design

All animal experiments were carried out according to the guidelines of the Volcani Center Institutional Committee for Care and Use of Laboratory Animals. Nude (CD1 nu/nu) male mice (Harlan Laboratories, Jerusalem, Israel) were housed in cages (4 mice per cage) under conditions of constant photoperiod (12-hour light/12-shour dark) with free access to food and water. In the first experiment, xenografts (n = 10/group) were established by implanting the human pancreatic cell line MiaPaca-2 with Matrigel, at 7.5 × 10^5 cells per mouse, subcutaneously (SC) on both flanks, using a 27-gauge needle. Halofuginone was injected intraperitoneally (IP) at 10 μg per mouse, 3 times per week, starting 8 days after cell implantation. In the second experiment, xenografts were established by implanting 10^6 MiaPaca-2 cells, with no Matrigel, with or without 5 × 10^5 PSCs derived from naive mice and from mice treated with a single IP injection of cerulein (50 μg/kg) for 24 hours. During both experiments, tumor size was determined with a caliper, according to the formula: length × width × depth ×

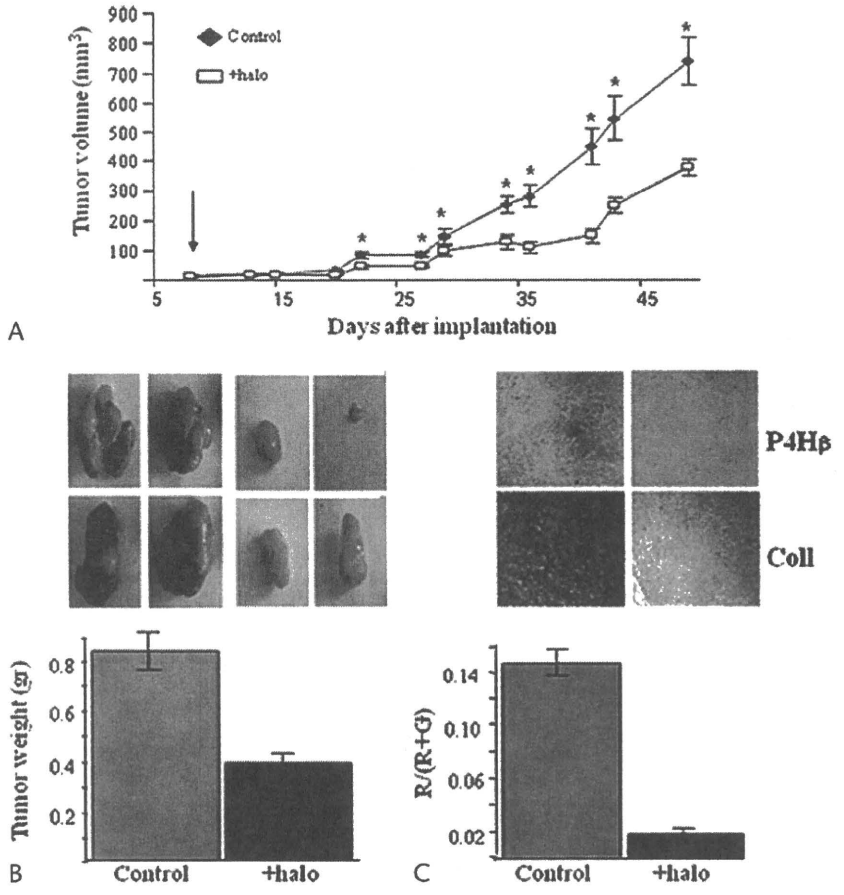

FIGURE 1. Effect of halofuginone on tumor progression. A, Pancreatic tumor cells were implanted SC on both flanks of CD1 nu/nu mice (n = 10), and halofuginone (10 μg/mouse) was injected IP 3 times a week starting 8 days after cell implantation (arrow). Tumor volume is expressed as the mean ± SE. Note that halofuginone treatment caused a significant reduction in tumor growth (*) from day 22 ($P < 0.05$ according to Duncan multiple range test). Tumor weight (B) and P4Hβ (C) (immunohistochemistry) and collagen (Sirius red staining) levels in the tumors on day 49 after cell implantation. Tumor weight of all tumors is expressed as the mean ± SE. The level of collagen was also quantified by image analysis, and the results were calculated as red (R) area divided by the total red + green (R + G) area of at least 20 photos taken from different mice for each analysis and presented as arbitrary units of the mean ± SE.

0.5236, and is presented as mean ± SE. In the orthotopic model, pancreatic fibrosis was induced by repeated 6-hourly IP injections of cerulein, at 50 μg/kg, twice weekly for 8 weeks,[36,49] and halofuginone was injected IP at 7.5 μg per mouse 3 times per week, starting at the same time as the cerulein. After 8 weeks, when pancreatic fibrosis was established, a dose of 2×10^6 MiaPaca-2 cells was injected directly into the spleen (n = 7), and after an additional 39 days, the animals were killed, and the pancreatic tissue was taken for assessment of tumor numbers by means of proliferating cell nuclear antigen staining. No mortality was observed in the control untreated mice or in those treated only with halofuginone, whereas 2 and 3 mice died from the groups treated with cerulein together with halofuginone and cerulein alone, respectively.

Preparation of Sections and Immunohistochemistry

At the end of the experiments, pancreatic tissue or tumors were collected and fixed overnight in 4% paraformaldehyde in phosphate-buffered saline at 4°C. Serial 5-μm sections were prepared and embedded in Paraplast (Shandan, Runcorn, United Kingdom)[37] and were stained with Sirius red for collagen. Collagen levels were quantified by image analysis with the ImagePro software (Media Cybernetics, Silver Spring, Md).[44] At least 20 photographs of tissue sections from different mice were taken for each analysis, and the results were calculated as red (R) area divided by the total red + green (R + G) area and presented as arbitrary units of the mean ± SE. Immunohistochemistry was performed with anti-Cygb/STAP and anti-P4Hβ antibodies at dilutions of 1:500 and 1:25, respectively. Peroxidase activity was revealed by using 3,3′-diaminobenzidine as chromogen.

Western Blot

Thirty-microgram samples of protein lysates were electrophoresed on 10% sodium dodecyl sulfate–polyacrylamide gel and transferred onto a nitrocellulose membrane. Nonspecific binding sites were blocked with 5% low-fat milk, and the membranes were incubated overnight with the appropriate Cygb/STAP (1:1000) antibodies.

RESULTS

Effect of Halofuginone on Tumor Growth

All MiaPaca-2 pancreatic tumor cells, when implanted SC with Matrigel rich in ECM proteins, resulted in tumors that reached a mean volume of 742 mm^3 and weight of 0.85 g on day 49 after cell implantation (Figs. 1A, B). Halofuginone administered 8 days after cell implantation did not affect the number of tumors formed but inhibited tumor development to an extent that was statistically significant as early as day 22; by day 49 after implantation, the tumor mean volume and weight were 371 mm^3 and 0.39 g, respectively. The tumors that developed in the

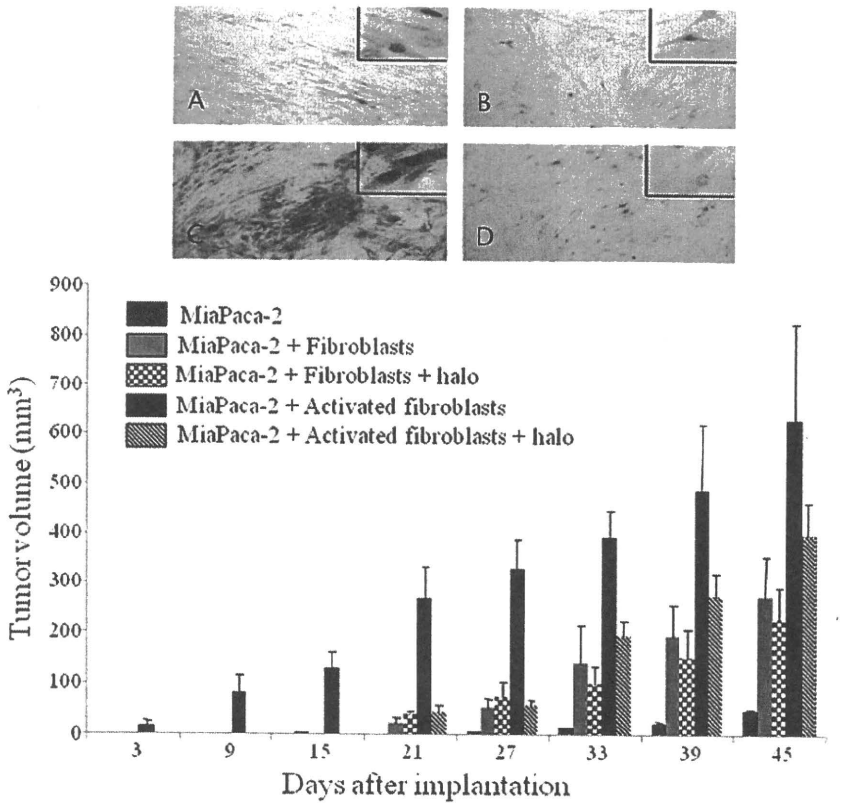

FIGURE 2. Pancreatic stellate cell activation and tumor growth. Upper panel, Cygb/STAP levels in (A) PSCs derived from pancreas of untreated mice, (B) PSCs derived from pancreas of untreated mice that were treated in vitro with halofuginone (25 nM, 48 hours), (C) PSCs derived from pancreas of cerulein-treated mice, and (D) PSCs derived from pancreas of cerulein-treated mice treated in vitro with halofuginone. Cygb/STAP levels as determined by immunohistochemistry. Lower panel, MiaPaca-2 tumor cells were implanted SC without Matrigel, alone, or with PSCs derived from untreated or cerulein-treated mice that had been pretreated with halofuginone before implantation (n = 8/group). Tumor volume was recorded periodically, and the results are expressed as the mean ± SE.

untreated mice contained high levels of collagen, organized in fibrils that encircled clusters of cancer cells and formed fibrous septae, and high levels of P4Hβ, a major collagen cross-linking enzyme that is used as a marker for activated fibroblasts (Fig. 1C). Almost no collagen or P4Hβ was observed in the halofuginone-treated tumors.

Activation of PSCs and Tumor Establishment and Growth

Pancreatic stellate cells were isolated from the pancreas of untreated and cerulein-treated mice and were incubated in vitro with or without 25 nM halofuginone for 48 hours. Low levels of Cygb/STAP were observed in cells isolated from the pancreas of untreated naive mice and were not affected by halofuginone (Fig. 2A). The cells isolated from the cerulein-treated mice exhibited a high level of Cygb/STAP, which was reduced by halofuginone to levels resembling those of the cells derived from the untreated mice. MiaPaca-2 tumor cells, when implanted SC alone without Matrigel, produced very few tumors (2/10 = 20%), and these developed slowly, were not detected until 27 days after implantation, and reached a mean volume of 48.4 mm^3 after 49 days (Fig. 2B). When implanted with PSCs derived from the pancreas of untreated mice, MiaPaca-2 tumor cells produced more tumors (16/20 = 80%), and these developed more rapidly, were detected on day 21 after implantation, and reached a mean volume of 270.2 mm^3 at the end of the experiment. Similar results were obtained when the pancreatic tumor cells were implanted with fibroblasts isolated from mouse peritoneum (data not shown). Pretreatment of the PSCs with halofuginone reduced the number of tumors formed (8/20 = 40%) without affecting the progress of the remaining tumors or their final volume. When the tumor cells were implanted together with PSCs derived from cerulein-treated mice that exhibited high levels of Cygb/STAP, almost the maximum number of tumors was achieved (19/20 = 95%). The tumors were detected as early as day 3 after implantation and reached a mean volume of 630.5 mm^3. Reductions in both tumor number (16/20 = 80%) and final tumor volume (to 396 mm^3) were observed when the cells derived from cerulein-treated mice were preincubated with halofuginone. At the end of the experiment—49 days after implantation—the tumors resulting from MiaPaca-2 cells implanted alone contained few cells that expressed Cygb/STAP (Fig. 3A). An increase in the numbers of cells expressing Cygb/STAP was observed in tumors derived from MiaPaca-2 cells implanted with PSCs from pancreas (Fig. 3B) or from peritoneum (Fig. 3C) of control untreated mice, and further increase was observed in tumors derived from MiaPaca-2 cells implanted together with cells from cerulein-treated mice (Fig. 3D). Preincubation of the PSCs with halofuginone caused reduction in the numbers of Cygb/STAP–expressing cells among those derived from either cerulein-untreated or cerulein-treated mice (Figs. 3E, F).

Fibrotic Pancreas, Tumor Establishment, and Development

Fibrosis in pancreas after cerulein treatment was evaluated by measuring collagen and Cygb/STAP levels. Cerulein treatment resulted in a major increase in the levels of pancreas collagen that surrounds the acinar cells (Fig. 4A) and of Cygb/STAP synthesized by activated PSCs (Figs. 4B, C). Halofuginone had no effect on the collagen content or Cygb/STAP levels in the untreated mice, but in the cerulein-treated mice, it reduced

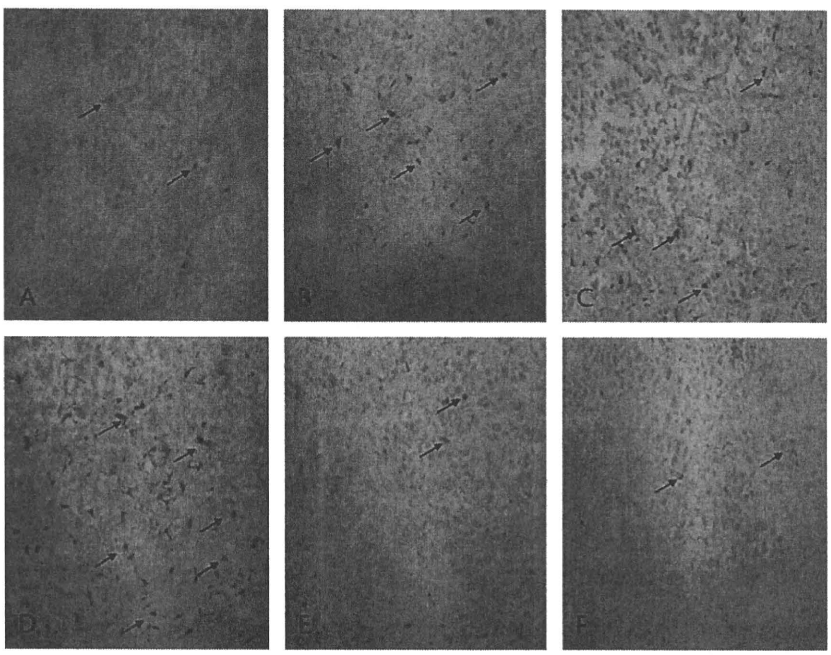

FIGURE 3. Evaluation of Cygb/STAP–expressing cells in tumors. MiaPaca-2 tumor cells were implanted SC without Matrigel, alone, or with PSCs derived from untreated or cerulein-treated mice that had been pretreated with halofuginone before implantation (n = 8/group). At the end of the experiment (49 days after implantation), the tumors were taken for immunohistochemistry and stained with Cygb/STAP antibodies. MiaPaca-2 alone (A), MiaPaca-2 together with PSCs from untreated mice (B), MiaPaca-2 together with fibroblast from peritoneum of untreated mice (C), MiaPaca-2 together with PSCs from cerulein-treated mice (D), MiaPaca-2 together with PSCs from untreated mice pretreated in vitro with halofuginone (E), and MiaPaca-2 together with PSCs from cerulein-treated mice pretreated in vitro with halofuginone (F).

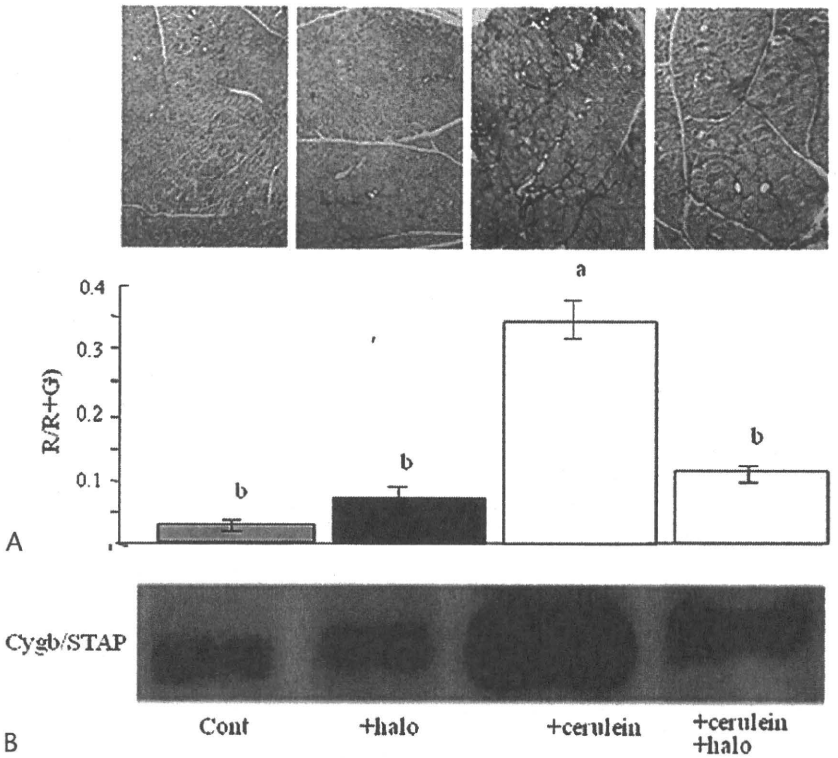

FIGURE 4. Effect of halofuginone on cerulein-dependent pancreatic fibrosis. Pancreatic fibrosis was induced by repeated 6-hourly IP injections of cerulein (50 μg/kg) twice weekly, with or without halofuginone (7.5 μg/mouse) that was injected IP 3 times a week starting at the same time as cerulein. After 8 weeks, pancreas tissue was taken (n = 8/group) for (A) collagen determination (Sirius red staining and image analysis); for image analysis, at least 20 photos were taken from different mice. According to Duncan multiple range test, the yellow column is significantly higher ($P < 0.05$) compared with all other columns. B, Evaluation of Cygb/STAP by Western blotting after equal protein loading.

both to levels that did not differ from those in the control untreated mice.

Injection of MiaPaca-2 tumor cells into the spleen resulted in very few tumors in the pancreas of the untreated mice, regardless of halofuginone treatment (Fig. 5), but when the tumor cells were injected into the spleen of the mice with cerulein-dependent pancreatic fibrosis, the number of tumors increased. Inhibition of the cerulein-dependent fibrosis by halofuginone resulted in reduction in the formation of pancreatic tumors to numbers that did not differ from those observed in the untreated mice.

DISCUSSION

When implanted with Matrigel, which contains a great excess of ECM components, all the malignant cells were able to produce tumors (Fig. 1). At this stage, halofuginone had no effect on the number of tumors formed, as was observed in other xenografts.[46,47] With time, as the Matrigel is dissolved by the tissue, tumor growth and development depend on the endogenous ECM produced by myofibroblasts, as indicated by the high levels of collagen and its cross-linking enzyme (Fig. 1C). These myofibroblasts may originate from mouse-skin-resident fibroblasts, or they may derive from a circulating fibroblast population, from the vascular bed, or from hemopoietic progenitor or stromal cells from the bone marrow.[50,51] In addition, epithelial cells of various tissues are an important source of myofibroblasts, and this transdifferentiation is a specialized version of the epithelial-mesenchymal transition, a process in which epithelial cells can acquire characteristics of mesenchymal cells.[52–54] It is important to note that, during fibrogenesis[55] and in the tumor microenvironment,[56] the myofibroblasts constitute heterogeneous populations of cells, probably derived from diverse origins, that express different sets of genes and that may have differing functions. The collagen observed in subcutaneous tumors implanted without any addition of fibroblasts is probably originated, at least in part, by mouse stroma cells. This is based on the following: (*a*) implantation of tumor cells to mice expressing green fluorescent protein revealed stroma mouse cells migrating into the tumor, and (*b*) using mouse-specific collagen type I antibodies, we could detect mouse collagen within the human tumor (data not shown). The differentiation of the stroma fibroblasts to myofibroblasts of various tumors and the activation of the PSCs in pancreatic cancer are probably induced by the tumors themselves.[3,24,25] By inhibiting fibroblast activation, halofuginone caused almost complete elimination of collagen synthesis and of the level of its major cross-linking enzyme within the tumors together with an inhibition of tumor growth and development. In the pancreatic cancer (Fig. 1), as well in other xenografts, such as prostate cancer, Wilms tumor, and renal cell carcinoma,[7,46,47] halofuginone had major effects on tumor growth. However, no complete arrest of the tumor growth was observed; rather, there was a significant delay in its progress. Because of its unique mode of action—that is, targeting the fibroblast-to-myofibroblast transition via inhibition of Smad3 phosphorylation—halofuginone synergizes with the

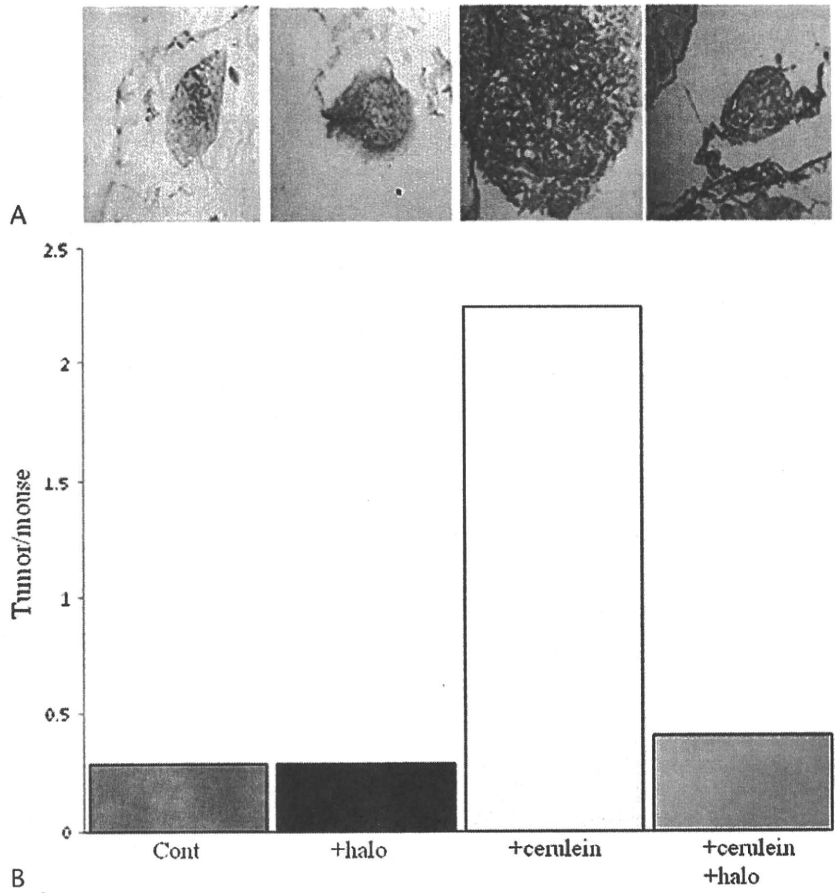

FIGURE 5. Pancreatic fibrosis and tumor establishment. Pancreatic fibrosis was induced by repeated 6-hourly IP injections of cerulein (50 μg/kg) twice weekly with or without halofuginone (7.5 μg/mouse) that was injected IP 3 times a week starting at the same time as cerulein. After 8 weeks, when pancreatic fibrosis was established, MiaPaca-2 cells (2×10^6 cells) were injected directly into the spleen (n = 7), and after an additional 39 days, the animals were killed, and the pancreas tissue was taken for assessment of (A) tumor collagen levels by Sirius Red staining and (B) tumor numbers. According to Duncan multiple range test, the yellow column is significantly higher ($P < 0.05$) compared with all other columns.

chemotherapy that affects the tumor cells, resulting in major reductions in tumor growth.[37]

In agreement with findings of other studies,[26] in the present study pancreatic tumor cells implanted SC alone without ECM produced few tumors, and these progressed slowly, whereas addition of PSCs to the implanted tumor cells resulted in more tumors, which progressed much faster (Fig. 2). The number of tumors produced and their rate of development did not depend solely on the presence of the PSCs, but also on their state of activation. Tumor cells that were implanted together with activated PSCs originated from cerulein-treated fibrotic pancreas that exhibited high levels of Cygb/STAP (Fig. 2A) and of transgelin (SMA22α)[36] resulted in larger numbers of tumors, which grew to larger volumes, than those that were implanted with PSCs from normal mice. Transforming growth factor β, probably secreted by the inflammatory cells, stimulates PSC activation and induces transcription of ECM proteins, mainly via phosphorylation of the Smad3.[57,58] By inhibiting Smad3 phosphorylation, halofuginone inhibits activation of stromal fibroblasts and of hepatic and PSCs.[34,36,37,41] Monitoring of Cygb/STAP levels (Fig. 2A) showed that inhibition of PSC activation by halofuginone before implantation with the tumor cells resulted in reductions in both the number of tumors developed and their growth rate. Suppression of Smad3 expression in activated PSCs led also to the loss of membrane-anchored MMP inhibitor (RECK) protein expression, which suggests that TGF-β signaling in activated PSCs may promote ECM accumulation, not only by increasing ECM production but also via a mechanism that preserves the protease inhibitory activity.[59] RECK expression is also under the control of pancreatitis-associated protein.[60] It is interesting to note that halofuginone increased the synthesis of PAP-1 by the acinar cells, which could further reduce PSC activation and pancreas fibrosis.[36] Tumors implanted with activated PSCs maintained high levels of Cygb/STAP–positive cells even 49 days after implantation (Fig. 3), which again suggests the presence of activated PSCs of various origins. Upon activation, the PSCs, in addition to ECM remodeling, have the ability to produce a wide variety of cytokines, chemokines, and growth factors such as interleukin (IL) 1β, IL-6, tumor necrosis factor α, IL-8, monocyte chemoattractant protein 1, TGF-β1, and platelet-derived growth factor BB, all of which contribute to perpetuation of PSC activation, recruitment of inflammatory cells to the inflamed pancreas, and to tumor development.

Cygb/STAP is probably involved in cellular oxygen homeostasis and serves as an O_2 reservoir under hypoxic

conditions. The hypoxia that occurs in fibrotic pancreas and in pancreatic tumors increases ECM production and synthesis of vascular endothelial growth factor by PSCs.[61] Cygb/STAP expression is upregulated under hypoxia, by hypoxia-inducible factor 1 (HIF-1).[62] Hypoxia-inducible factor 1 expression is correlated with the fibrotic focus in ductal adenocarcinoma, and the aberrant ECM production is essential for tumor angiogenesis.[63] The inhibition of angiogenesis by halofuginone[46,47,64] may suggest the involvement, at least in part, of HIF-1–dependent Cygb/STAP overexpression in angiogenesis and tumor development.

The accumulation of ECM in cases of chronic pancreatitis and pancreatic cancer not only accompanies both diseases but also is directly involved in their progress and has a significant impact on patient survival.[65] After spleen injection of tumor cells, more tumors were developed in the fibrotic pancreas than in the control (Fig. 5). Inhibition of fibroblast activation, as indicated by the presence of fewer Cygb/STAP–expressing cells, and reduction of collagen content to control levels by halofuginone (Fig. 4) resulted in reduction in the number of tumors formed (Fig. 5). Halofuginone did not affect collagen synthesis or Cygb/STAP levels in the control mice. This finding confirms our previous observations that, in most animal models of fibrosis, regardless of the tissue, halofuginone had a minimal effect on collagen content in the control, nonfibrotic animals, whereas it exhibited a profound inhibitory effect in the TGF-β–dependent fibrotic organs.[41] These results suggest a different regulation of the housekeeping genes and usually low level of collagen synthesis in normal tissue on the one hand and an aggressive and a rapid process during tissue fibrosis on the other hand.

Recently, halofuginone was found to activate a cytoprotective signaling pathway—the amino acid starvation response—that is, a potent and selective regulator of inflammatory T-cell differentiation.[66] When amino acids are limiting, a protective starvation response program is initiated in which translation of most RNAs into proteins is blocked, and the expression of a selective set of protective genes is induced. This response involves activation of GCN2 (general control nonderepressible 2) and PERK (pancreatic endoplasmic reticulum eIF2α) kinases, which inactivate the eukaryotic translation initiation factor 2α. Consequently, translation of most RNAs is turned off. However, these conditions favor the translation of RNA encoding ATF4 (activating transcription factor 4), which induces expression of specific protective genes.[67–70] Whether amino acid starvation response is part of, or required for, PSC activation remains to be elucidated.

In conclusion, the activated PSCs seem to be the key elements in the cross-talk between the parenchymal cells and the desmoplastic stroma. The ECM produced by these cells is involved both in the establishment of the malignant cells within the tissue and in the development of the tumor. These results suggest that targeting the PSC activation might become a promising therapeutic approach for which there is a great unmet need.

REFERENCES

1. van Kempen LC, Ruiter DJ, van Muijen GN, et al. The tumor microenvironment: a critical determinant of neoplastic evolution. *Eur J Cell Biol.* 2003;82:539–548.
2. Shekhar MPV, Pauley R, Heppner G. Host microenvironment in breast cancer development: extracellular matrix–stromal cell contribution to neoplastic phenotype of epithelial cells in the breast. *Breast Cancer Res.* 2003;5:130–135.
3. Zalatnai A. Molecular aspects of stromal-parenchymal interactions in malignant neoplasms. *Curr Mol Med.* 2006;6:685–693.
4. Ronnov-Jessen L, Villadsen R, Edwards JC, et al. Differential expression of a chloride intracellular channel gene, CLIC4, in transforming growth factor-beta1–mediated conversion of fibroblasts to myofibroblasts. *Am J Pathol.* 2002;161:471–480.
5. Lewis MP, Lygoe KA, Nystrom ML, et al. Tumour-derived TGF-beta1 modulates myofibroblast differentiation and promotes HGF/SF-dependent invasion of squamous carcinoma cells. *Br J Cancer.* 2004;90:822–832.
6. Micke P, Ostman A. Tumour-stroma interaction: cancer-associated fibroblasts as novel targets in anti-cancer therapy? *Lung Cancer.* 2004;45(suppl 2):S163–S175.
7. Genin O, Rechavi G, Nagler A, et al. Myofibroblasts in pulmonary and brain metastases of alveolar soft-part sarcoma: a novel target for treatment? *Neoplasia.* 2008;10:940–948.
8. Kalluri R, Zeisberg M. Fibroblasts in cancer. *Nat Rev Cancer.* 2006;6:392–401.
9. DeClerck YA. Interactions between tumour cells and stromal cells and proteolytic modification of the extracellular matrix by metalloproteinases in cancer. *Eur J Cancer.* 2000;36:1258–1268.
10. De Wever O, Mareel M. Role of myofibroblasts at the invasion front. *Biol Chem.* 2002;383:55–67.
11. Tuxhorn JA, Ayala GE, Smith MJ, et al. Reactive stroma in human prostate cancer: induction of myofibroblast phenotype and extracellular matrix remodeling. *Clin Cancer Res.* 2002;8:2912–2923.
12. Zidar N, Gale N, Kambic V, et al. Proliferation of myofibroblasts in the stroma of epithelial hyperplastic lesions and squamous carcinoma of the larynx. *Oncology.* 2002;62:381–385.
13. Armstrong T, Packham G, Murphy LB, et al. Type I collagen promotes the malignant phenotype of pancreatic ductal adenocarcinoma. *Clin Cancer Res.* 2004;10:7427–7437.
14. van Hoorde L, van Aken E, Mareel M. Collagen type I: a substrate and a signal for invasion. *Prog Mol Subcell Biol.* 2000;25:105–134.
15. Lockwood DS, Yeadon TM, Clouston AD, et al. 2003 Tumor progression in hepatocellular carcinoma: relationship with tumor stroma and parenchymal disease. *J Gastroenterol Hepatol.* 2003;18:666–672.
16. Vaquero EC, Edderkaoui M, Nam KJ, et al. Extracellular matrix proteins protect pancreatic cancer cells from death via mitochondrial and nonmitochondrial pathways. *Gastroenterology.* 2003;125:1188–1202.
17. Apte MV, Wilson JS. Mechanisms of pancreatic fibrosis. *Dig Dis.* 2004;22:273–279.
18. Jaster R. Molecular regulation of pancreatic stellate cell function. *Mol Cancer.* 2004;3:26–34.
19. Glass A, Kundt G, Brock P, et al. Delayed response toward activation stimuli in pancreatic stellate cells. *Pancreas.* 2006;33:293–300.
20. Bachem MG, Schunemann M, Ramadani M, et al. Pancreatic carcinoma cells induce fibrosis by stimulating proliferation and matrix synthesis of stellate cells. *Gastroenterology.* 2005;128:907–921.
21. Erkan M, Kleeff J, Gorbachevski A, et al. Periostin creates a tumor-supportive microenvironment in the pancreas by sustaining fibrogenic stellate cell activity. *Gastroenterology.* 2007;132:1447–1464.
22. Omary MB, Lugea A, Lowe AW, et al. The pancreatic stellate cell: a star on the rise in pancreatic diseases. *J Clin Invest.* 2007;117:50–59.
23. Hwang RF, Moore T, Arumugam T, et al. Cancer-associated stromal fibroblasts promote pancreatic tumor progression. *Cancer Res.* 2008;68:918–926.
24. Vonlaufen A, Joshi S, Qu C, et al. Pancreatic stellate cells: partners in crime with pancreatic cancer cells. *Cancer Res.* 2008a;68:2085–2093.
25. Vonlaufen A, Phillips PA, Xu Z, et al. Pancreatic stellate cells and pancreatic cancer cells: an unholy alliance. *Cancer Res.* 2008b;68:7707–7710.
26. Bachem MG, Zhou S, Buck K, et al. Pancreatic stellate cells-role in pancreas cancer. *Langenbecks Arch Surg.* 2008;393:891–900.
27. Schneider G, Siveke JT, Eckel F, et al. Pancreatic cancer: basic and clinical aspects. *Gastroenterology.* 2005;128:1606–1625.

28. Cohen SJ, Alpaugh RK, Palazzo I, et al. Fibroblast activation protein and its relationship to clinical outcome in pancreatic adenocarcinoma. *Pancreas*. 2008;37:154–158.
29. Truty MJ, Urrutia R. Basics of TGF-beta and pancreatic cancer. *Pancreatology*. 2007;7:423–435.
30. Mahadevan D, Von Hoff DD. Tumor-stroma interactions in pancreatic ductal adenocarcinoma. *Mol Cancer Ther*. 2007;6:1186–1197.
31. Nakatani K, Okuyama H, Shimahara Y, et al. Cytoglobin/STAP, its unique localization in splanchnic fibroblast-like cells and function in organ fibrogenesis. *Lab Invest*. 2004;84:91–101.
32. Fordel E, Thijs L, Martinet W, et al. Neuroglobin and cytoglobin overexpression protects human SH-SY5Y neuroblastoma cells against oxidative stress-induced cell death. *Neurosci Lett*. 2006;410:146–151.
33. Xu R, Harrison PM, Chen M, et al. Cytoglobin overexpression protects against damage-induced fibrosis. *Mol Ther*. 2006;13:1093–1100.
34. Bruck R, Genina O, Aeed H, et al. Halofuginone to prevent and treat thioacetamide-induced liver fibrosis in rats. *Hepatology*. 2001;3:379–386.
35. Gnainsky Y, Kushnirsky Z, Bilu G, et al. Gene expression during chemically induced liver fibrosis: effect of halofuginone on TGF-beta signaling. *Cell Tiss Res*. 2007;328:153–166.
36. Zion O, Genin O, Kawada N, et al. Inhibition of transforming growth factor beta signaling by halofuginone as a modality for pancreas fibrosis prevention. *Pancreas*. 2009;38:427–435.
37. Sheffer Y, Leon O, Pinthus JH, et al. Inhibition of fibroblast to myofibroblast transition by halofuginone contributes to the chemotherapy-mediated antitumoral effect. *Mol Cancer Ther*. 2007;6:570–577.
38. McGaha TL, Phelps RG, Spiera H, et al. Halofuginone, an inhibitor of type-I collagen synthesis and skin sclerosis, blocks transforming-growth-factor-beta–mediated Smad3 activation in fibroblasts. *J Invest Dermatol*. 2002;118:461–470.
39. Xavier S, Piek E, Fujii M, et al. Amelioration of radiation-induced fibrosis: inhibition of transforming growth factor-beta signaling by halofuginone. *J Biol Chem*. 2004;279:15167–15176.
40. Yee KO, Connolly CM, Pines M, et al. Halofuginone inhibits tumor growth in the polyoma middle T antigen mouse via a thrombospondin-1 independent mechanism. *Cancer Biol Ther*. 2006;5:218–224.
41. Pines M. Targeting TGFβ signaling to inhibit fibroblasts activation as a therapy for fibrosis and cancer. *Expert Opin Drug Dis*. 2008;3:11–20.
42. Levi-Schaffer F, Nagler A, Slavin S, et al. Inhibition of collagen synthesis and changes in skin morphology in murine graft-versus-host disease and tight skin mice: effect of halofuginone. *J Invest Dermatol*. 1996;106:84–88.
43. Pines M, Domb A, Ohana M, et al. Reduction in dermal fibrosis in the tight-skin (Tsk) mouse after local application of halofuginone. *Biochem Pharmacol*. 2001;62:1221–1227.
44. Turgeman T, Hagai Y, Huebner K, et al. Prevention of muscle fibrosis and improvement in muscle performance in the mdx mouse by halofuginone. *Neuromuscul Disord*. 2008;18:857–868.
45. Abramovitch R, Dafni H, Neeman M, et al. Inhibition of neovascularization, tumor growth and facilitation of wound repair by halofuginone, an inhibitor of collagen type I synthesis. *Neoplasia*. 1999;1:321–329.
46. Gavish Z, Pinthus JH, Barak V, et al. Growth inhibition of prostate cancer xenografts by halofuginone. *Prostate*. 2002;51:73–83.
47. Pinthus JH, Sheffer Y, Nagler A, et al. Inhibition of Wilms tumor xenografts progression by halofuginone is accompanied by activation of WT1 gene expression. *J Urol*. 2005;174:1527–1531.
48. Kruse ML, Hildebrand PB, Timke C, et al. Isolation, long-term culture, and characterization of rat pancreatic fibroblastoid/stellate cells. *Pancreas*. 2001;23:49–54.
49. Neuschwander-Tetri BA, Burton FR, Presti ME, et al. Repetitive self-limited acute pancreatitis induces pancreatic fibrogenesis in the mouse. *Dig Dis Sci*. 2000;45:665–674.
50. Hast J, Schiffer IB, Neugebauer B, et al. Angiogenesis and fibroblast proliferation precede formation of recurrent tumors after radiation therapy in nude mice. *Anticancer Res*. 2002;22:677–688.
51. Ogawa M, LaRue AC, Drake CJ. Hematopoietic origin of fibroblasts/myofibroblasts: its pathophysiologic implications. *Blood*. 2006;108:2893–2896.
52. Radisky DC, Kenny PA, Bissell MJ. Fibrosis and cancer: do myofibroblasts come also from epithelial cells via EMT? *J Cell Biochem*. 2007;101:830–839.
53. Acloque H, Adams MS, Fishwick K, et al. Epithelial-mesenchymal transitions: the importance of changing cell state in development and disease. *J Clin Invest*. 2009;119:1438–1449.
54. Kalluri R, Weinberg RA. The basics of epithelial-mesenchymal transition. *J Clin Invest*. 2009;119:1420–1428.
55. Magness ST, Battaler R, Yang L, et al. A dual reporter gene transgenic mouse demonstrates heterogeneity in hepatic fibrogenic cell populations. *Hepatology*. 2004;40:1151–1159.
56. Sugimoto H, Mundel TM, Kieran MW, et al. Identification of fibroblast heterogeneity in the tumor microenvironment. *Cancer Biol Ther*. 2006;5:1640–1646.
57. Talukdar R, Tandon RK. Pancreatic stellate cells: new target in the treatment of chronic pancreatitis. *J Gastroenterol Hepatol*. 2008;23:34–41.
58. Ellenrieder V, Schneiderhan W, Bachem M, et al. Fibrogenesis in the pancreas. *Rocz Akad Med Bialymst*. 2004;49:40–46.
59. Lee H, Lim C, Lee J, et al. TGF-beta signaling preserves RECK expression in activated pancreatic stellate cells. *J Cell Biochem*. 2008;104:1065–1074.
60. Li L, Bachem MG, Zhou S, et al. Pancreatitis-associated protein inhibits human pancreatic stellate cell MMP-1 and -2, TIMP-1 and -2 secretion and RECK expression. *Pancreatology*. 2009;9:99–110.
61. Erkan M, Reiser-Erkan C, Michalski CW, et al. Cancer-stellate cell interactions perpetuate the hypoxia-fibrosis cycle in pancreatic ductal adenocarcinoma. *Neoplasia*. 2009;11:497–508.
62. Schmidt M, Gerlach F, Avivi A, et al. Cytoglobin is a respiratory protein in connective tissue and neurons, which is up-regulated by hypoxia. *J Biol Chem*. 2004;279:8063–8069.
63. Couvelard A, O'Toole D, Leek R, et al. Expression of hypoxia-inducible factors is correlated with the presence of a fibrotic focus and angiogenesis in pancreatic ductal adenocarcinomas. *Histopathology*. 2005;46:668–676.
64. Elkin M, Miao HQ, Nagler A, et al. Halofuginone: a potent inhibitor of critical steps in angiogenesis progression. *FASEB J*. 2000; 14:2477–2485.
65. Erkan M, Michalski CW, Rieder S, et al. The activated stroma index is a novel and independent prognostic marker in pancreatic ductal adenocarcinoma. *Clin Gastroenterol Hepatol*. 2008;6:1155–1161.
66. Sundrud MS, Koralov SB, Feuerer M, et al. Halofuginone inhibits T_H17 cell differentiation by activating the amino acid starvation response. *Science*. 2009;324:1334–1338.
67. Deval C, Chaveroux C, Maurin AC, et al. Amino acid limitation regulates the expression of genes involved in several specific biological processes through GCN2-dependent and GCN2-independent pathways. *FEBS J*. 2009;276:707–718.
68. Harding HP, Novoa I, Zhang Y, et al. Regulated translation initiation controls stress-induced gene expression in mammalian cells. *Mol Cell*. 2000;6:1099–1108.
69. Wek RC, Jiang HY, Anthony TG. Coping with stress: eIF2 kinases and translational control. *Biochem Soc Trans*. 2006;34:7–11.
70. Blander MJ, Amsen D. Amino acid addiction. *Science*. 2009;324:1282–1283.

Emerging Antiviral Drugs for Hepatitis C Virus

Masaru Enomoto, Akihiro Tamori and Norifumi Kawada*

Department of Hepatology, Osaka City University Medical School, Osaka, Japan

Abstract: Infection with hepatitis C virus (HCV) is a global health problem that affects approximately 170 million people worldwide. The current standard therapy with peginterferon alpha plus ribavirin for 48 weeks results in a sustained virologic response in less than 50% of patients with chronic hepatitis C genotype 1—the most prevalent type of HCV in North America and Europe. Development of new antiviral medicines has been hampered by the lack of an effective cell culture system and small-animal model. Herein we review recent progress in the development of new treatments under investigation in clinical trials, including specifically targeted antiviral therapy for HCV such as NS3/4A protease and NS5B polymerase inhibitors.

Keywords: Hepatitis C virus, interferon, polymerase inhibitor, protease inhibitor, ribavirin, STAT-C.

INTRODUCTION

Hepatitis C virus (HCV), a member of the family *Flaviviridae*, infects approximately 170 million people worldwide and is an important health care problem [1]. Persistent infection with HCV often progresses to chronic hepatitis, liver cirrhosis, and possibly hepatocellular carcinoma over the course of several decades. The current standard therapy with peginterferon alpha and ribavirin for 48 weeks results in a sustained virologic response (SVR), defined as undetectable HCV RNA levels 24 weeks after the end of therapy, in less than 50% of patients with chronic hepatitis C genotype 1—the most prevalent type of HCV in North America and Europe [2, 3]. No effective alternative treatment is currently available for non-responders.

Until recently, development of new antiviral medicines has been hampered by the lack of an effective cell culture system and small-animal model. In 1999, Lohmann *et al.* reported selection of the first functional subgenomic replicons in cell culture [4]. In 2005, Wakita *et al.* showed that the full-length JFH-1 genome, a genotype 2a HCV isolate obtained from a patient in Japan with fulminant hepatitis, produces infectious particles in cell culture [5]. On the other hand, a chimeric mouse model for human liver diseases has been established by transplanting normal human hepatocytes into severe combined immunodeficiency mice carrying a plasminogen activator transgene [6]. These experimental systems provide important tools for evaluating potential antiviral compounds.

As shown in Fig. (**1**), the HCV genome consists of a 9.6-kb uncapped linear single-stranded RNA with positive polarity [7]. It contains 5′ and 3′ untranslated regions including control elements required for translation and replication. The untranslated regions flank an uninterrupted open reading frame encoding a single polyprotein of 3,010 amino acids, which is processed into structural (C, E1, E2, and p7) and nonstructural (NS2, NS3, NS4A, NS4B, NS5A, and NS5B) subunits. The HCV NS3/4A serine protease or NS5B RNA-dependent RNA polymerase is essential for viral replication and can be specific targets of new antiviral agents. In fact, these agents have shown a potent antiviral effect, but monotherapy has been complicated by rapid virologic breakthrough due to the selection of drug-resistant mutants [8,9]. The efficacy of most specifically targeted antiviral therapies for HCV (STAT-C) is therefore focused on a combination of peginterferon alpha and ribavirin. *In vitro* resistance profiles for point mutations within the HCV NS3 protease and NS5B polymerase are shown in Fig. (**2**). Drug-resistant mutations limit subsequent treatment options because of cross-resistance.

We herein review recent progress in the development of new treatments under investigation in clinical trials, including STAT-C agents such as NS3/4A protease and NS5B polymerase inhibitors.

INTERFERON FORMULATION

Interferon alpha is a key drug for the treatment of chronic HCV infection. It initiates the Janus kinase/signal transducer and activates the transcription signaling cascade, which leads to the transcriptional induction of interferon-stimulated genes and subsequently establishes a non-specific antiviral state within the cell [10]. The attachment of a polyethyleneglycol moiety to interferon alpha produces a biologically active molecule with a long half-life and favorable pharmacokinetics. Peginterferon alpha is administered weekly as a current standard of care in combination with ribavirin [2, 3].

Albinterferon alpha-2b is a novel 85.7-kDa recombinant polypeptide consisting of interferon alpha-2b that is genetically fused to human serum albumin. The albumin-fusion platform takes advantage of the long half-life of human albumin to provide a new treatment approach that allows a reduction in the dosing frequency of interferon alpha [11]. The Phase IIa study examined the use of two subcutaneous injections of albinterferon alpha-2b 14 days apart, at doses ranging from 200 to 1,200 μg, and showed that the median terminal half-life extended to 141 h, that is longer than half-life of peginterferon alpha (approximately 40–80 h) [12]. Albinterferon alpha-2b was well tolerated at doses up to 1,200 μg, and the mean reduction in HCV RNA at week 4 in

*Address Correspondence to this author at the Department of Hepatology, Graduate School of Medicine, Osaka City University Medical School, 1-4-3 Asahimachi, Abeno-ku, Osaka 545-8585, Japan; Tel: 81-6-6645-3811; Fax: 81-6-6645-3813; E-mail: kawadanori@med.osaka-cu.ac.jp

1574-8871/08 $55.00+.00

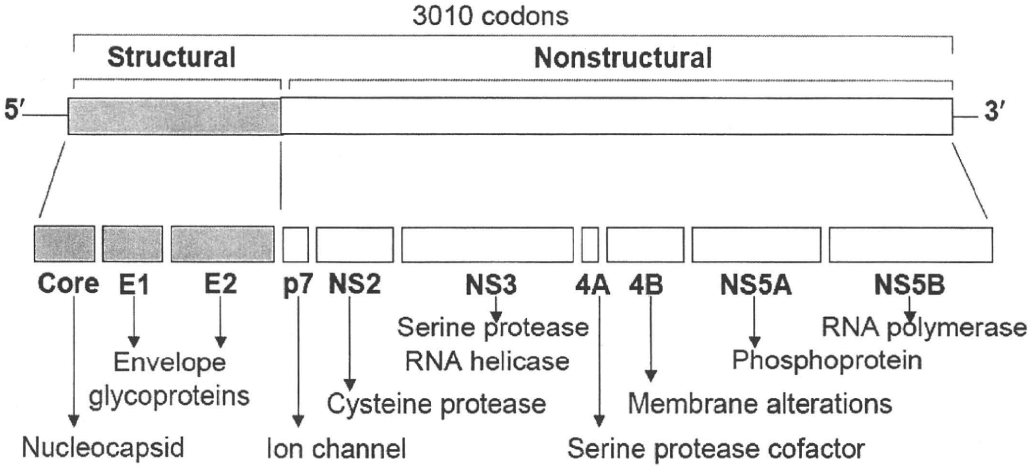

Fig. (1). Structure of the HCV genome. It consists of approximately 9,600 nucleotides in positive, single-stranded RNA, including the long open reading frame, encoding a single polyprotein of 3,010 amino acids which is processed into structural (C, E1, E2, and p7) and nonstructural (NS2, NS3, NS4A, NS4B, NS5A, and NS5B) subunits, and 5′ and 3′ untranslated regions.

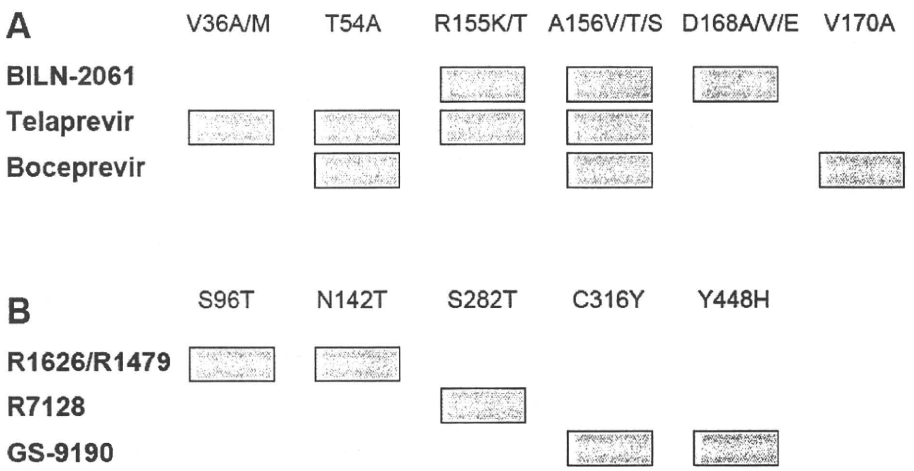

Fig. (2). *In vitro* resistance profiles for point mutations within the HCV NS3 protease (**A**) and NS5B polymerase (**B**). The list does not contain all identified variants.

those given the higher doses of 900 or 1,200 μg was 3.2 $\log_{10}$ IU/mL. In the Phase IIb study, previously untreated (naïve) patients with genotype 1 chronic hepatitis C were randomly assigned to a 48-week treatment with 180 μg peginterferon alpha-2a once per week, 900 or 1,200 μg albinterferon alpha-2b once every 2 weeks, or 1,200 μg albinterferon alpha-2b once every 4 weeks plus weight-based ribavirin [13]. The rates of SVR by intention-to-treat analysis ranged from 51% to 59% in the 3 albinterferon groups treated at 2- or 4-week intervals compared with 58% in the weekly peginterferon group ($P = 0.64$ for overall test).

RIBAVIRIN DERIVATIVE

Ribavirin is a synthetic guanosine nucleoside analogue that inhibits the replication of various RNA and DNA viruses. Although the exact mechanisms by which ribavirin could act in HCV infection remains uncertain, some mechanisms have been proposed, including immunomodulation promoting T helper cell type 1 over type 2 phenotype, inosine monophosphate dehydrogenase inhibition leading to GTP depletion, direct inhibition of HCV RNA polymerase, and mutagenesis resulting in reduced virion infectivity [10]. Monotherapy with ribavirin was associated with improvements in aminotransferase levels in at least half of the patients with chronic hepatitis C, but not with a significant decrease in serum HCV RNA levels. However, the addition of ribavirin to interferon results in a substantially higher rate of SVR than does interferon alone [14, 15].

Hemolytic anemia is the most common reason for reducing the dose and discontinuing ribavirin, which can lower the efficacy of treatment [16]. Administration of erythropoietin can improve anemia caused by ribavirin, but is associated

with additional costs, inconvenience, and potential side effects. Taribavirin (Viramidine), a liver-targeted prodrug of ribavirin, is associated with a lower incidence of anemia [17]. In the Phase II randomized study of taribavirin versus ribavirin combined with peginterferon alpha-2a in treatment-naïve patients with chronic hepatitis C, the rate of SVR did not differ significantly between the taribavirin (23%, 37% and 29% at 800, 1200, and 1600 mg) and ribavirin (44% at 1000 and 1200 mg) groups. Fewer patients receiving taribavirin (4%) than ribavirin (27%) had severe anemia (hemoglobin <10 g/dL).

NS3/4A SERINE PROTEASE INHIBITORS

BILN-2061

BILN-2061 was the first NS3/4A protease inhibitor to be examined. Administration of 200 mg BILN-2061 twice daily for 2 days resulted in an impressive effect that corresponds to a reduction in plasma HCV RNA levels of 2 to 3 $\log_{10}$ or greater for all treated patients with genotype 1 infection [18]. However, development was halted because of cardiac toxicity in laboratory animals.

Telaprevir (VX-950)

Telaprevir is an inhibitor specific to the HCV NS3/4A serine protease. In a Phase I randomized trial of 750 mg telaprevir 3 times daily with and without peginterferon alpha-2a in previously untreated patients with genotype 1 hepatitis C, the median change in HCV RNA from baseline to day 15 was -1.09 $\log_{10}$ in the placebo group, -3.99 $\log_{10}$ in the telaprevir group, and -5.49 $\log_{10}$ in the telaprevir and peginterferon alpha-2a group [19].

In Phase II randomized clinical trials known as the PROVE 1 and 2 Studies, conducted in patients with chronic HCV genotype 1 infection who had not been treated previously, the triple-therapy group that received telaprevir (1250 mg on day 1 and 750 mg every 8 hours thereafter), peginterferon alpha-2a, and ribavirin for 12 weeks followed by peginterferon alpha-2a and ribavirin for 12 more weeks (total 24 weeks) had significantly higher rates of SVR (61–69%) than did the standard-therapy group that received peginterferon alpha-2a and ribavirin for 48 weeks (41–46%) [20, 21]. However, viral breakthrough occurred in 7% of patients who received telaprevir. The rate of discontinuation because of adverse events, including pruritus, rash, and anemia, was higher in the groups who received telaprevir.

The interim analysis of the Phase II clinical trial PROVE3, conducted in patients with HCV genotype 1 infection who previously failed treatment with peginterferon alpha and ribavirin, showed that the rates of SVR in the triple-therapy group (telaprevir, peginterferon alpha-2a, and ribavirin for 12 weeks followed by peginterferon alpha-2a and ribavirin for 12 more weeks for a total of 24 weeks) was 51% compared with 14% in the standard-therapy group (peginterferon alpha-2a and ribavirin for 48 weeks) [22].

Boceprevir (SCH 503034)

Boceprevir is another oral HCV NS3/4A protease inhibitor. In the Phase I study, boceprevir plus peginterferon alpha-2b was well tolerated in patients with HCV genotype 1 infection who were previously nonresponders to peginterferon alpha-2b with or without ribavirin [23]. Mean maximum $\log_{10}$ changes in HCV RNA were -2.88 by treatment with peginterferon alpha-2b plus 400 mg boceprevir 3 times daily for 2 weeks compared with -1.08 to -1.26 by treatment with peginterferon alpha-2b alone for 2 weeks.

In the Phase II clinical trial known as HCV SPRINT-1, the triple-therapy group that received peginterferon alpha-2b and ribavirin for 4 weeks (lead-in) followed by the addition of 400 mg boceprevir 3 times daily to the combination for 24 or 44 weeks (total 28 or 48 weeks) had significantly higher rates of SVR (56–75%) than did the 48-week standard-therapy group (38%), which consisted of treatment-naïve patients with chronic HCV genotype 1 infection [24]. Of interest, introduction of a 4-week lead-in with the standard therapy before the addition of boceprevir reduced the incidence of viral breakthrough. The incidence of rash-related adverse events was similar with the boceprevir-containing regimens and the control. Treatment discontinuations due to adverse events, including anemia, nausea, and headache, were 9–19% in the boceprevir arms compared with 8% in the control arm.

TMC435 (TMC435350-C201)

Interim results from the Phase II clinical trial OPERA-1 showed that 75 or 200 mg of the protease inhibitor TMC435 once daily, in combination with peginterferon alpha-2a and ribavirin, decreased HCV RNA levels to below the lower limit of quantification (<25 IU/mL) on day 28 in all treatment-naïve patients with HCV genotype 1 who were assigned to the triple-therapy arms [25]. The trial is ongoing for treatment-experienced patients.

R7227/ITMN-191

In the Phase I multiple ascending dose study, the protease inhibitor R7227/ITMN-191 reduced HCV RNA in a dose dependent manner through day 14 [26]. Treatment with 200 mg of R7227/ITMN-191 3 times daily resulted in rapid and sustained reductions in HCV RNA, with a median reduction of 3.8 $\log_{10}$ at day 14. The rate of treatment response was lower in prior non-responders than in treatment-naïve HCV genotype 1 patients.

NUCLEOSIDE POLYMERASE INHIBITORS

R1626

R1626 is a prodrug of the nucleoside inhibitor of HCV NS5B polymerase R1479. In the Phase II clinical trial in HCV genotype 1–infected treatment-naïve patients, triple therapy with peginterferon alpha-2a and ribavirin plus 1500 mg R1626 twice daily resulted in a rapid virologic response (defined as an undetectable HCV RNA level at week 4) in 74% of patients compared with 5% of patients receiving standard therapy with peginterferon alpha-2a and ribavirin [27]. However, development was recently discontinued because of hematological toxicity issues and a high relapse rate [28].

R7128

R7128 is a prodrug of the nucleoside inhibitor of HCV NS5B polymerase PSI-6130. The interim results of the Phase I clinical trial showed that R7128 delivered a rapid virologic response in 85–88% of treatment-naïve patients with HCV genotype 1 infection, compared with 10% with the standard of care, when administered at doses of 1000 to 1500 mg twice daily in combination with peginterferon alpha-2a and ribavirin for 28 days [29]. The high rate of rapid virologic response (≥86%) was also reported in HCV genotype 2/3 non-responders [30].

NON-NUCLEOSIDE POLYMERASE INHIBITORS

Filibuvir (PF-00868554)

Filibuvir is a non-nucleoside inhibitor of HCV NS5B polymerase. Interim 4-week results of the Phase I clinical trial in treatment-naïve patients with chronic hepatitis C genotypes 1 showed that the addition of 200, 300, and 500 mg Filibuvir twice daily for the first 4 weeks of peginterferon alpha-2a and ribavirin treatment resulted in a rapid virologic response in 60%, 75% and 63% of patients, respectively, compared with 0% with peginterferon alpha-2a and ribavirin [31].

GS-9190

GS-9190 is also a non-nucleoside HCV NS5B polymerase inhibitor. In the Phase I dose-escalation trial in treatment-naïve patients with chronic HCV genotypes 1, 40–240 mg GS-9190 was well tolerated, and reductions in individual HCV RNA levels ranged from 0.19 to 2.54 $\log_{10}$ after single-dose exposure [32]. In the multiple dose cohort, however, a possible but not confirmed QT elongation was observed. The trial to study the safety and effectiveness of GS-9190 in combination with peginterferon alpha-2a and ribavirin is ongoing.

ANA598

In the Phase I multiple ascending dose trial in treatment-naïve patients with chronic HCV genotypes 1, a non-nucleoside polymerase inhibitor ANA598 dosed 200 mg twice daily for 3 days as monotherapy demonstrated potent antiviral activity with median viral load decline of 2.4 $\log_{10}$ [33].

NS5A INHIBITOR

BMS790052

BMS790052 is a first-in-class and highly selective HCV NS5A inhibitor. The function of NS5A remains to be poorly understood, but increasing evidence implicates NS5A in multiple essential functions, including modifying the interferon response, facilitating RNA replication, and assembling the virus. In the Phase I ascending-dose study in treatment-naïve or experienced patients with genotype 1 chronic hepatitis C, mean decline in HCV RNA 24 hours after a single 1, 10 and 100 mg dose of BMS790052 was 1.8 $\log_{10}$, 3.2 $\log_{10}$ and 3.3 $\log_{10}$, respectively. Multiple dose trials are ongoing [34].

HOST-TARGETED DRUGS

Nitazoxanide

Nitazoxanide is a member of the thiazolide class of antiparasitic drugs and is licensed in the United States for the treatment of *Cryptosporidium parvum* and *Giardia lamblia*. HCV genotype 4 is the predominant type in the Middle East and Africa, particularly Egypt, and is insensitive to interferon therapy, as is genotype 1. In the Phase II trial conducted in Egypt [35], SVR rates were significantly higher in previously untreated patients with chronic hepatitis C genotype 4 infection given 500 mg nitazoxanide twice daily for 12 weeks followed by nitazoxanide plus peginterferon alpha-2a and ribavirin for 36 weeks (total 48 weeks) than in those treated with peginterferon alpha-2a and ribavirin for 48 weeks (79% compared with 50%; $P = 0.023$). Adverse events were similar across treatment groups. Although the exact mechanism of action remains unknown, *in vitro* nitazoxanide may result in the activation of the double-stranded RNA-activated protein kinase—a key mediator of host cell defenses [36].

Debio-025

Cyclosporin A inhibits the replication of HCV subgenomic replicons. This antiviral effect is not mediated by its immunosuppressive action, but by blockade of intracellular ligands of cyclosporin A, the cyclophilins [37]. Debio-025 is an oral, non-immunosuppressive cyclophilin inhibitor derived from cyclosporin A that has more potent anti-HCV activity than does cyclosporin A in *in vitro* subgenomic replicons and in *in vivo* chimeric mice models [38, 39]. The Phase II trial [40] showed, in treatment-naïve patients with chronic hepatitis C genotypes 1 and 4, that 600 and 1,000 mg Debio-025 per day in combination with peginterferon alpha-2a induced continuous decays in viral load at week 4 that reached –4.61 and –4.75 $\log_{10}$, respectively, compared with –2.49 $\log_{10}$ by peginterferon alpha-2a alone. Headache, nausea, fatigue, and hyperbilirubinemia were the most frequent treatment-emergent adverse events, but no serious events were reported.

CONCLUSIONS

Many novel antiviral agents for HCV are now under clinical investigation. However, any single agent cannot lead to sustained viral eradication. In particular, STAT-C agents cause the rapid selection of drug-resistant mutants when used alone. At present, combination therapy with peginterferon alpha and ribavirin is necessary to reduce the incidence of viral breakthrough and to raise the SVR rate. It is also important to establish measures to overcome safety issues, because the addition of some STAT-C agents to the current standard of care is sometimes associated with a higher rate of treatment discontinuation because of adverse events. In the future, the safety and efficacy of combining multiple direct antiviral agents from different classes should be established,

as for highly active antiretroviral treatment of human immunodeficiency virus infection. The Phase I trial INFORM-1 to study the safety, efficacy and pharmacokinetics of combination of protease inhibitor R7227/ITMN-191 and nucleoside polymerase inhibitor R7128 is currently underway [41].

REFERENCES

[1] Shepard CW, Finelli L, Alter MJ. Global epidemiology of hepatitis C virus infection. *Lancet Infect Dis* 2005; 5: 558–67.

[2] Manns MP, McHutchison JG, Gordon SC, Rustgi VK, Shiffman M, Reindollar R, Goodman ZD, Koury K, Ling M, Albrecht JK. Peginterferon alfa-2b plus ribavirin compared with interferon alfa-2b plus ribavirin for initial treatment of chronic hepatitis C: a randomised trial. *Lancet* 2001; 358: 958–65.

[3] Fried MW, Shiffman ML, Reddy KR, Smith C, Marinos G, Gonçales FL Jr, Häussinger D, Diago M, Carosi G, Dhumeaux D, Craxi A, Lin A, Hoffman J, Yu J. Peginterferon alfa-2a plus ribavirin for chronic hepatitis C virus infection. *N Engl J Med* 2002; 347: 975–82.

[4] Lohmann V, Körner F, Koch J, Herian U, Theilmann L, Bartenschlager R. Replication of subgenomic hepatitis C virus RNAs in a hepatoma cell line. *Science* 1999; 285: 110–3.

[5] Wakita T, Pietschmann T, Kato T, Date T, Miyamoto M, Zhao Z, Murthy K, Habermann A, Kräusslich HG, Mizokami M, Bartenschlager R, Liang TJ. Production of infectious hepatitis C virus in tissue culture from a cloned viral genome. *Nat Med* 2005; 11: 791–6.

[6] Mercer DF, Schiller DE, Elliott JF, Douglas DN, Hao C, Rinfret A, Addison WR, Fischer KP, Churchill TA, Lakey JR, Tyrrell DL, Kneteman NM. Hepatitis C virus replication in mice with chimeric human livers. *Nat Med* 2001; 7: 927–33.

[7] Chisari FV. Unscrambling hepatitis C virus-host interactions. *Nature* 2005; 436: 930–2.

[8] Thompson AJ, McHutchison JG. Antiviral resistance and specifically targeted therapy for HCV (STAT-C). *J Viral Hepat* 2009; 16: 377–87.

[9] Soriano V, Peters M, Zeuzem S. New therapies for hepatitis C virus infection. *Clin Infect Dis* 2009; 48: 313–20.

[10] Feld JJ, Hoofnagle JH. Mechanism of action of interferon and ribavirin in treatment of hepatitis C. *Nature* 2005; 436: 967–72.

[11] Subramanian GM, Fiscella M, Lamousé-Smith A, Zeuzem S, McHutchison JG.. Albinterferon alpha-2b: a genetic fusion protein for the treatment of chronic hepatitis C. *Nat Biotechnol* 2007; 25: 1411–9.

[12] Bain VG, Kaita KD, Yoshida EM, Swain MG, Heathcote EJ, Neumann AU, Fiscella M, Yu R, Osborn BL, Cronin PW, Freimuth WW, McHutchison JG, Subramanian GM. A phase 2 study to evaluate the antiviral activity, safety, and pharmacokinetics of recombinant human albumin-interferon alfa fusion protein in genotype 1 chronic hepatitis C patients. *J Hepatol* 2006; 44: 671–8.

[13] Zeuzem S, Yoshida EM, Benhamou Y, Pianko S, Bain VG, Shouval D, Flisiak R, Rehak V, Grigorescu M, Kaita K, Cronin PW, Pulkstenis E, Subramanian GM, McHutchison JG. Albinterferon alfa-2b dosed every two or four weeks in interferon-naïve patients with genotype 1 chronic hepatitis C. *Hepatology* 2008; 48: 407–17.

[14] Reichard O, Norkrans G, Frydén A, Braconier JH, Sönnerborg A, Weiland O. Randomised, double-blind, placebo-controlled trial of interferon alpha-2b with and without ribavirin for chronic hepatitis C. Swedish Study Group. *Lancet* 1998; 351: 83–7.

[15] Davis GL, Esteban-Mur R, Rustgi V, Hoefs J, Gordon SC, Trepo C, Shiffman ML, Zeuzem S, Craxi A, Ling MH, Albrecht J. Interferon alfa-2b alone or in combination with ribavirin for the treatment of relapse of chronic hepatitis C. International Hepatitis Interventional Therapy Group. *N Engl J Med* 1998; 339: 1493–9.

[16] McHutchison JG, Manns MP, Brown RS Jr, Reddy KR, Shiffman ML, Wong JB. Strategies for managing anemia in hepatitis C patients undergoing antiviral therapy. *Am J Gastroenterol* 2007; 102: 880–9.

[17] Gish RG, Arora S, Rajender Reddy K, Nelson DR, O'Brien C, Xu Y, Murphy B. Virological response and safety outcomes in therapy-naïve patients treated for chronic hepatitis C with taribavirin or ribavirin in combination with pegylated interferon alfa-2a: a randomized, phase 2 study. *J Hepatol* 2007; 47: 51–9.

[18] Lamarre D, Anderson PC, Bailey M, Beaulieu P, Bolger G, Bonneau P, Bös M, Cameron DR, Cartier M, Cordingley MG, Faucher AM, Goudreau N, Kawai SH, Kukolj G, Lagacé L, LaPlante SR, Narjes H, Poupart MA, Rancourt J, Sentjens RE, St George R, Simoneau B, Steinmann G, Thibeault D, Tsantrizos YS, Weldon SM, Yong CL, Llinàs-Brunet M. An NS3 protease inhibitor with antiviral effects in humans infected with hepatitis C virus. *Nature* 2003; 426: 186–9.

[19] Forestier N, Reesink HW, Weegink CJ, McNair L, Kieffer TL, Chu HM, Purdy S, Jansen PL, Zeuzem S. Antiviral activity of telaprevir (VX-950) and peginterferon alfa-2a in patients with hepatitis C. *Hepatology* 2007; 46: 640–8.

[20] McHutchison JG, Everson GT, Gordon SC, Jacobson IM, Sulkowski M, Kauffman R, McNair L, Alam J, Muir AJ; PROVE1 Study Team. Telaprevir with peginterferon and ribavirin for chronic HCV genotype 1 infection. *N Engl J Med* 2009; 360: 1827–38.

[21] Hézode C, Forestier N, Dusheiko G, Ferenci P, Pol S, Goeser T, Bronowicki JP, Bourlière M, Gharakhanian S, Bengtsson L, McNair L, George S, Kieffer T, Kwong A, Kauffman RS, Alam J, Pawlotsky JM, Zeuzem S; PROVE2 Study Team. Telaprevir and peginterferon with or without ribavirin for chronic HCV infection. *N Engl J Med* 2009; 360: 1839–50.

[22] Manns M, Muir A, Adda N, Jacobson I, Afdhal N, Heathcote J, Zeuzem S, Reesink H, Terrault N, Bsharat M, George S, McHutchison J, Di Bisceglie A. Telaprevir in hepatitis C genotype-1-infected patients with prior non-response, viral breakthrough or relapse to peginterferon-alfa-2a/b and ribavirin therapy: SVR results of the PROVE3 study. *J Hepatol* 2009; 50 (Suppl 1): S379.

[23] Sarrazin C, Rouzier R, Wagner F, Forestier N, Larrey D, Gupta SK, Hussain M, Shah A, Cutler D, Zhang J, Zeuzem S. SCH 503034, a novel hepatitis C virus protease inhibitor, plus pegylated interferon alpha-2b for genotype 1 nonresponders. *Gastroenterology* 2007; 132: 1270–8.

[24] Kwo P, Lawitz E, McCone J, Schiff E, Vierling J, Pound D, Davis M, Galati J, Gordon S, Ravendhran N, Rossaro L, Anderson F, Jacobson I, Rubin R, Koury K, Brass C, Chaudhri E, Albrecht J. HCV SPRINT-1 final results: SVR 24 from a phase 2 study of boceprevir plus pegIntron (peginterferon alfa-2b)/ribavirin in treatment-naïve subjects with genotype 1 chronic hepatitis C. *J Hepatol* 2009; 50 (Suppl 1): S4.

[25] Manns M, Reesink H, Moreno C, Berg T, Benhamou Y, Horsmans Y, Dusheiko G, Flisiak R, Meyvisch P, Lenz O, Sekar V, van't Klooster G, Simmen K, Verloes R. Opera-1 Trial: Interim analysis of safety and antiviral activity of TMC435 in treatment-naïve genotype 1 HCV patients. *J Hepatol* 2009; 50 (Suppl 1): S7.

[26] Forestier N, Larrey DG, Guyader D, Marcellin P, Rouzier R, Patat AA, Bradford WZ, Porter S, Zeuzem S. Treatment of chronic hepatitis C virus (HCV) genotype 1 patients with the NS3/4A protease inhibitor ITMN-191 leads to rapid reductions in plasma HCV RNA: results of a rhase 1b multiple ascending dose (MAD) study. *Hepatology* 2008; 48 (Suppl): 1132A.

[27] Pockros PJ, Nelson D, Godofsky E, Rodriguez-Torres M, Everson GT, Fried MW, Ghalib R, Harrison S, Nyberg L, Shiffman ML, Najera I, Chan A, Hill G. R1626 plus peginterferon alfa-2a provides potent suppression of hepatitis C virus RNA and significant antiviral synergy in combination with ribavirin. *Hepatology* 2008; 48: 85–97.

[28] Pockros P, Nelson D, Godofsky E, Rodriguez-Torres M, Everson GT, Fried MW, Ghalib R, Harrison S, Nyberg L, Shiffman ML, Chan A, Hill G. High relapse rate seen at week 72 for patients treated with R1626 combination therapy. *Hepatology* 2008; 48: 1349–50.

[29] Rodriguez-Torres M, Lalezari J, Gane EJ, DeJesus E, Nelson DR, Everson GT, Jacobson IM, Reddy KR, McHutchison JG, Beard A, Walker S, Symonds W, Berrey MM. Potent antiviral response to the HCV nucleoside polymerase inhibitor R7128 for 28 days with peg-IFN and ribavirin: subanalysis by race/ethnicity, weight and HCV genotype. *Hepatology* 2008; 48 (Suppl): 1160A.

[30] Gane EJ, Rodriguez-Torres M, Nelson DR, Jacobson IM, McHutchison JG, Jeffers L, Beard A, Walker S, Shulman N, Symonds W, Albanis E, Berrey MM. Antiviral activity of the HCV

nucleoside polymerase inhibitor R7128 in HCV genotype 2 and 3 prior non-responders: interim results of R7128 1500 mg BID with PEG-IFN and ribavirin for 28 days. *Hepatology* 2008; 48 (Suppl): 1024A.

[31] Jacobson I, Pockros P, Lalezari J, Lawitz E, Rodriguez-Torres M, DeJesus E, Haa F, Martorell C, Pruitt R, Durham K, Srinivasan S, Rosario M, Jagannatha S, Hammond J. Antiviral activity of filibuvir in combination with pegylated interferon alfa-2a and ribavirin for 28 days in treatment-naïve patients chronically infected with HCV genotype 1. *J Hepatol* 2009; 50 (Suppl 1): S382–3.

[32] Bavisotto L, Wang CC, Jacobson IM, Marcellin P, Zeuzem S, Lawitz EJ, Lunde M, Sereni P, O'Brien C. Antiviral, pharmacokinetic and safety data for GS-9190, a non-nucleoside HCV NS5b polymerase inhibitor, in a phase-1 trial in HCV genotype 1 infected subjects. *Hepatology* 2007; 46 (Suppl): 255A.

[33] Lawitz E, Rodriguez-Torres M, DeMico M, Nguyen T, Godofsky E, Appleman J, Rahimy M, Crowley C, Freddo J. Antiviral activity of ANA598, a potent non-nucleoside polymerase inhibitor, in chronic hepatitis C patients. *J Hepatol* 2009; 50 (Suppl 1): S384.

[34] Nettles R, Chien C, Chung E, Persson A, Gao M, Belema M, Meanwell NA, DeMicco MP, Marbury TC, Goldwater R, Northup P, Coumbis J, Kraft WK, Charlton MR, Lopez-Talavero JC, Grasela D. BMS-790052 is a first-in-class potent hepatitis C virus (HCV) NS5A inhibitor for patients with chronic HCV infection: results from a proof-of-concept study. *Hepatology* 2008; 48 (Suppl): 1025A.

[35] Rossignol JF, Elfert A, El-Gohary Y, Keeffe EB. Improved virologic response in chronic hepatitis C genotype 4 treated with nitazoxanide, peginterferon, and ribavirin. *Gastroenterology* 2009; 136: 856–62.

[36] Elazar M, Liu M, McKenna SA, Liu P, Gehrig EA, Puglisi JD, Rossignol JF, Glenn JS. The anti-hepatitis C agent nitazoxanide induces phosphorylation of elongation initiation factor 2alpha via protein kinase activated by double-stranded RNA activation. *Gastroenterology* 2009 in press.

[37] Nakagawa M, Sakamoto N, Tanabe Y, Koyama T, Itsui Y, Takeda Y, Chen CH, Kakinuma S, Oooka S, Maekawa S, Enomoto N, Watanabe M. Suppression of hepatitis C virus replication by cyclosporin a is mediated by blockade of cyclophilins. *Gastroenterology* 2005; 129: 1031–41.

[38] Paeshuyse J, Kaul A, De Clercq E, Rosenwirth B, Dumont JM, Scalfaro P, Bartenschlager R, Neyts J. The non-immunosuppressive cyclosporin DEBIO-025 is a potent inhibitor of hepatitis C virus replication in vitro. *Hepatology* 2006; 43: 761–70.

[39] Inoue K, Umehara T, Ruegg UT, Yasui F, Watanabe T, Yasuda H, Dumont JM, Scalfaro P, Yoshiba M, Kohara M. Evaluation of a cyclophilin inhibitor in hepatitis C virus-infected chimeric mice in vivo. *Hepatology* 2007; 45: 921–8.

[40] Flisiak R, Feinman SV, Jablkowski M, Horban A, Kryczka W, Pawlowska M, Heathcote JE, Mazzella G, Vandelli C, Nicolas-Métral V, Grosgurin P, Liz JS, Scalfaro P, Porchet H, Crabbé R. The cyclophilin inhibitor Debio 025 combined with PEG IFNalpha2a significantly reduces viral load in treatment-naïve hepatitis C patients. *Hepatology* 2009; 49: 1460–8.

[41] Gane EJ, Roberts SK, Stedman C, Angus PW, Ritchie B, Elston R, Ipe D, Baher L, Morcos P, Najera I, Mannino M, Brennan B, Berrey M, Bradford W, Yetzer E, Shulman N, Smith PF. First-in-man demonstration of potent antiviral activity with a nucleoside polymerase inhibitor (R7128) and protease (R7227/ITMN-191) inhibitor combination in HCV: safety, pharmacokinetics and virologic results from INFORM-1. *J Hepatol* 2009; 50 (Suppl 1): S380.

Received: July 21, 2009 Revised: September 26, 2009 Accepted: September 29, 2009

Laboratory Investigation (2010) 90, 245–256

Reversibility of fibrosis, inflammation, and endoplasmic reticulum stress in the liver of rats fed a methionine–choline-deficient diet

Yong-ping Mu[1,2], Tomohiro Ogawa[1] and Norifumi Kawada[1]

Fatty liver disease has become a health problem related to metabolic syndrome worldwide, although its molecular pathogenesis requires further study. It is also unclear whether advanced fibrosis of steatohepatitis will regress when diet is controlled. The aim of this study was to investigate whether the resolution of fibrosis occurs in steatohepatitis induced by a methionine–choline-deficient diet (MCDD). Manifestation of endoplasmic reticulum (ER) stress in this model was also studied. Nonalcoholic steatohepatitis with advanced fibrosis was induced in rats by feeding them an MCDD for 10 weeks. Instead of MCDD, a methionine–choline control diet (CD) was given for the last 2 weeks to the experimental group. Fibrosis and inflammation were determined by tissue staining. Protein and gene expressions were determined by immunoblotting and quantitative reverse transcription-PCR (RT-PCR), respectively. Expressions of caspase-7, caspase-12, glucose-regulated protein 78 (GRP78), and protein disulfide isomerase were evaluated to clarify the presence of ER stress. Changing the diet from MCDD to CD triggered the reduction of fat in hepatocytes, a decrease in inflammatory gene expression and oxidative stress, and regression of fibrosis accompanied by the disappearance of activated stellate cells and macrophages. Immunohistochemistry, immunoblotting, and RT-PCR analysis all indicated the occurrence of ER stress in steatohepatitis, while it recovered immediately after changing the diet from MCCD to CD. The ratio of hepatocyte proliferation/apoptotis increased significantly during the recovery stage. This simple experiment clearly shows that changing the diet from MCDD to a normal diet (CD) triggers the resolution of hepatic inflammatory and fibrotic reactions and hepatocyte apoptosis, suggesting that MCDD-induced steatohepatitis is also reversible. ER stress appears and disappears in association with the generation and regression of steatohepatitis, respectively, with fibrosis.
Laboratory Investigation (2010) **90,** 245–256; doi:10.1038/labinvest.2009.123; published online 30 November 2009

KEYWORDS: caspase; cytoglobin; hepatic stellate cells; hepatocytes; Kupffer cells; oxidative stress

Nonalcoholic fatty liver disease (NAFLD) is a relatively newly defined hepatic sequela of obesity and type II diabetes mellitus,[1–3] and it is one of the most common causes of chronic liver disease in many countries.[4] A number of studies have identified a significant correlation between hepatic steatosis and fibrosis.[5–7] NAFLD covers a progressive spectrum of liver pathologies from simple steatosis to nonalcoholic steatohepatitis (NASH), which is characterized by necroinflammation and fibrosis, and, subsequently, by cirrhosis.[8] It is also speculated that NASH may progress to hepatocellular carcinoma.[9–11]

Although adipocytokines, cytokines, and free fatty acids (FFAs) derived from peripheral and visceral fat tissues, which are known as mediators of metabolic syndrome, are assumed to contribute to the initiation of inflammatory reactions in the liver, the link between the development of hepatic steatosis and fibrosis is still poorly understood.[12] Furthermore, whether the regression of liver fibrosis caused by NASH occurs after controlling diet has not been proven, but the reversibility of liver fibrosis has been evidenced in patients who have successfully achieved the eradication of hepatitis C virus after interferon therapy.[13,14]

Over the past decade, it has become clear that obesity is associated with the activation of cellular stress signaling and inflammatory pathways.[15–17] A key cell organelle in cellular stress response is the endoplasmic reticulum (ER), a membranous network that functions in the synthesis and processing of secreted and membranous proteins. Certain

[1]Department of Hepatology, Graduate School of Medicine, Osaka City University, Osaka, Japan and [2]Shanghai Public Health Clinical Centre, Shanghai, China
Correspondence: Dr N Kawada, MD, PhD, Department of Hepatology, Osaka City University, Graduate School of Medicine, 1-4-3, Asahimachi, Abeno, Osaka 545-8585, Japan.
E-mail: kawadanori@med.osaka-cu.ac.jp

Received 26 March 2009; revised 2 September 2009; accepted 10 September 2009

pathological stress conditions disrupt ER homeostasis and lead to the accumulation of unfolded or misfolded proteins in the ER lumen, known as ER stress, resulting in the activation of signal transduction systems.[18–20] ER stress is caused by glucose or nutrient deprivation, viral infections, lipids, increased synthesis of secretory proteins, and expression of mutant or misfolded proteins, and has been recently implicated in human diseases, such as Alzheimer's disease, Parkinson's disease, diabetes mellitus, and liver disease.[21–24]

In this study, a rat steatohepatitis model induced by a methionine–choline-deficient diet (MCDD) for 10 weeks was used to obtain evidence for the resolution of fibrosis in fatty liver after changing the diet to a methionine–choline control diet (CD). The manifestation of ER stress was also studied. The results of this study clearly indicated that a dietary change from MCDD to CD immediately initiates tissue remodeling, which is associated with the cessation of cellular apoptosis and ER stress.

MATERIALS AND METHODS

Materials

Mouse monoclonal antibody against α-smooth muscle actin (α-SMA, Clone 1A4) and mouse monoclonal antibody against 5-bromo-2-deoxyuridine (BrdU, Clone 1BU33, 1:1000) were obtained from Sigma Chemical (St Louis, MO, USA). Rat monoclonal antibody against caspase-12 and goat polyclonal antibodies against glucose-regulated protein 78 (GRP78) were purchased from Santa Cruz Biotechnology (Santa Cruz, CA, USA). Rabbit polyclonal antibodies against caspase-7, rabbit polyclonal antibodies against cleaved caspase-7 (Asp198), and rabbit polyclonal antibodies against protein disulfide isomerase (PDI) were obtained from Cell Signaling Technology (Danvers, MA, USA). Mouse monoclonal antibody against CD68 (Clone, KP1) was purchased from Dako Denmark A/S (Glostrup, Denmark). Mouse monoclonal antibody against heme oxygenase-1 (HO-1, Hsp32) was obtained from Assay Designs (Ann Arbor, MI, USA). Mouse monoclonal antibody against 4-hydroxy-2-nonenal (4-HNE) was purchased from the Japan Institute for the Control of Aging (Shizuoka, Japan). Mouse monoclonal antibody against glyceraldehyde-3-phosphate dehydrogenase (GAPDH) was obtained from Chemicon International (Temecula, CA, USA). Rabbit anti-cytoglobin antibodies were produced in our laboratory as described previously.[25] Horseradish peroxidase (HRP)-conjugated polyclonal rabbit anti-goat immunoglobulins, HRP-conjugated polyclonal rabbit anti-mouse immunoglobulins, HRP-conjugated polyclonal rabbit anti-rat immunoglobulins, and HRP-conjugated polyclonal swine anti-rabbit immunoglobulins were obtained from Dako Denmark A/S. Hybond-ECL nitrocellulose membranes and ECL detection reagent were obtained from Amersham Pharmacia Biotech (Buckinghamshire, UK). All other reagents were purchased from Sigma Chemical or Wako Pure Chemical.

Animals and Experimental Protocol

Pathogen-free male Wistar rats (7–8 weeks of age) were obtained from SLC (Shizuoka, Japan). Animals were housed at a constant temperature and supplied with laboratory chow and water *ad libitum*. The experimental protocol was approved by the Animal Research Committee of Osaka City University (Guide for Animal Experiments, Osaka City University).

The rats were fed a CD (group C, $n=5$) or MCDD (group M, $n=5$) for 10 weeks. The contents of MCDD and CD are listed in Supplementary Table 1. A recovery model (group R, $n=5$) was produced by administering MCDD for 8 weeks and thereafter CD for 2 weeks. During the experimental period, individual body weights were recorded twice per week (see Supplementary Table 2).

Sample Harvesting

At the end of the tenth week, rats were killed under ether anesthesia, and the portal vein was cannulated using an 18-G Teflon catheter. Blood samples were collected from the inferior vena cava, centrifuged at 3000 r.p.m. for 30 min at 4°C, and the obtained sera were kept at −70°C until further use for serum chemistry tests. The liver of each animal was perfused with 100 ml of phosphate-buffered saline (pH 7.0) to remove blood and then washed with ice-cold saline, dried using filter paper, and weighed in a wet state. A portion of the liver was fixed with 4% paraformaldehyde, embedded in paraffin, and frozen. Another portion of the liver was snap-frozen in liquid nitrogen and stored at −70°C until use for reverse transcription-PCR (RT-PCR) and immunoblots.

Serum Chemistries

Serum levels of alanine aminotransferase (ALT), aspartate aminotransferase (AST), triglycerides (TGs), and FFAs were measured at Special Reference Laboratories (Osaka, Japan).

Histochemical and Immunohistochemical Analyses of the Rat Liver

Paraformaldehyde-fixed specimens were cut into 5-μm-thick sections and stained for 1 h with 0.1% (w/v) Sirius Red (Direct Red 80; Aldrich, Milwaukee, WI, USA), Oil red O, or hematoxylin and eosin (H&E). Immunohistochemistry was performed according to the methods described elsewhere.[26] Briefly, sections were deparaffinized, washed, and pre-incubated in blocking solution, followed by incubation with anti-4-HNE (15 μg/ml), HO-1 (1:50), CD68 (1:100), α-SMA (1:100), cytoglobin (1:400), or caspase-12 (1:100) antibodies. Sections were then incubated with HRP-conjugated secondary antibodies (1:1000), washed, covered with DAB, and counterstained with hematoxylin. Some of the immunostainings were performed at the Biopathology Institute (Oita, Japan). The red area on Oil red O staining was image analyzed by LuminaVision (Mitani Corporation, Tokyo, Japan).

TdT-Mediated dUTP Nick-End Labeling Assays

For the detection of apoptotic cells, paraffin-embedded sections were stained with the TdT-Mediated dUTP Nick-End Labeling (TUNEL) technique using an *In Situ* Apoptosis Detection kit (Takara Shuzo, Ohtsu, Japan) according to the manufacturer's instructions. For semi-quantitative analysis, the number of TUNEL-positive cells was counted in five randomly selected fields by viewing each slide at a magnification of × 400, and the average number in each group was calculated, as described previously.[27]

BrdU Assay for Hepatocyte Proliferation

For the detection of hepatocyte proliferation, rats were i.p. injected with BrdU (100 μg/kg) 2 h before being killed. *In situ* detection of the incorporation of BrdU into the nuclei was conducted immunohistochemically.[28] For semi-quantitative analysis, as for TUNEL, the number of BrdU-positive cells was counted in five randomly selected fields by viewing each slide at a magnification of × 200, and the average number in each group was calculated.

Quantitative RT-PCR

mRNA expressions of tumor necrosis factor-alpha (TNF-α), transforming growth factor-beta 1 (TGF-β1), α-SMA, collagen 1A2 (COL1A2), matrix metalloproteinases (MMPs)-2, -9, and -13, tissue inhibitor of MMP-1 (TIMP-1), caspases-3, -7, -9, and -12, GRP78, interleukin-6 (IL-6), BAX, BAK, Bcl-xl, Bcl-2, and ERp57 were assessed by quantitative RT-PCR. Total RNA was extracted from liver tissues using Isogen (Nippon Gene, Tokyo, Japan).[29] The expression of mRNA was measured using TaqMan One-Step RT-PCR Master Mix Reagents (Applied Biosystems, Foster City, CA, USA) or using the One-Step SYBR RT-PCR Kit (Perfect Real Time; Takara Bio, Ohtsu, Japan), and Applied Biosystems Prism 7700 (Applied Biosystems) according to a previously reported procedure.[27] Primers and oligonucleotide probes were designed using Primer Express (Sigma Chemical), and are listed in Table 1. Each PCR amplification was performed on five rats in both experimental and control groups. Individual gene expression was normalized by GAPDH. The conditions for the TaqMan One-Step RT-PCR were as follows: 30 min at 48°C (stage 1, RT), 10 min at 95°C (stage 2, RT inactivation and Ampli Taq Gold activation), and then 40 cycles of amplification for 15 s at 95°C and 1 min at 60°C (stage 3, PCR). The conditions for the One-Step SYBR RT-PCR (Perfect Real Time) were as follows: an initial step of 15 min at 42°C, 2 min at 95°C, and then 40 amplification cycles of denaturation at 95°C for 15 s, and annealing and extension at 60°C for 1 min.

Immunoblot Analysis

Some protein levels were assessed by immunoblot analysis, as described previously.[29] The liver tissue was lysed by RIPA buffer containing 50 mM Tris-HCl (pH 7.2), 150 mM NaCl, 1% NP-40, 0.1% SDS, 1 mM EDTA, and 1 mM PMSF and then homogenized in ice-cold water. After centrifugation for 10 min at 4°C and 12 000 r.p.m., the protein concentration of the obtained supernatant was determined using the Bio-Rad Dc protein Assay Reagent (Bio-Rad, Hercules, CA, USA). Protein was electrophoretically resolved in 10 or 12% SDS polyacrylamide gel, and successively transferred to Hybond-ECL nitrocellulose membranes. The membranes were blocked by 5% non-fat dietary milk solution in Tris-buffered saline (20 mM Tris and 150 mM NaCl, pH 7.4) with 0.1% Tween-20. They were then incubated overnight with primary antibodies at 4°C and successively with secondary antibodies at room temperature for 1 h. The following dilutions of primary antibodies were used: mouse monoclonal antibody to α-SMA, 1:1000; rabbit polyclonal antibodies to cytoglobin, 1:200; rat monoclonal antibody to caspase-12, 1:200; goat polyclonal antibodies to GRP78, 1:200; rabbit polyclonal antibodies to caspase-7, 1:1000; rabbit polyclonal antibodies to cleaved caspase-7 (Asp198), 1:1000; rabbit polyclonal antibodies against PDI, 1:200; mouse monoclonal antibody to GAPDH, 1:30 000. Immune complexes were visualized using a SuperSignal West Pico Chemiluminescent Substrate (ECL, Pierce, Rockford, IL, USA). Finally, band intensity was determined by scanning video densitometry.

Statistical Analysis

All results are expressed as mean ± s.d. Statistical analysis was performed using Student's *t*-test ($P<0.05$ was considered significant).

RESULTS

Accumulation of Fat in the Liver and Recovery after Dietary Change

As shown in Figure 1a and b, Oil red O staining clearly indicated that the MCDD diet (group M) for 10 weeks induced fat accumulation in the liver, especially in hepatocytes. It was also recognized that fat accumulation immediately decreased in group R ($P<0.01$), whose diet was changed from MCDD to CD during the last 2 weeks. The serum level of FFA was reduced in group M (183 ± 31.6 μequiv./l) compared with control group C (274 ± 35.7 μequiv./l) and recovery group R (267 ± 36.5 μequiv./l) ($P<0.01$). Similarly, the serum level of TG was reduced in group M (4.33 ± 1.21 mg/dl) compared with control group C (23.5 ± 4.95 mg/dl) and group R (28.2 ± 4.97 mg/dl) ($P<0.01$) (Figure 1c and d, $P<0.01$). Changes in the body weights of rats in each group are presented in Supplementary Table 2.

Liver Histology and Kupffer Cell Activation

H&E staining showed that the livers in group C showed an intact tissue structure, whereas those in group M showed the apparent vacuolization of hepatocytes, focal necrosis, and inflammatory cell accumulation in the parenchyma. These pathological changes were clearly improved in group R (Figure 2a). In accordance with this histological recovery, serum levels of AST and ALT were reduced from 97.7 ± 13.5

Table 1 Primer pairs and probes used for real-time PCR

Primer name	*Sequence*	*Note*
TNF-α		TaqMan
Forward	5′-GCT CCC TCT CAT CAG TTC CAT G-3′	
Reverse	5′-TAC GGG CTT GTC ACT CGA GTT TTG-3′	
Probe	5′-CCC AGA CCC TCA CAC TCA GAT CAT CTT C-3′	
Heme oxygenase-1		SYBR Green
Forward	5′-CGT GGC AGT GGG AAT TTA TG-3′	
Reverse	5′-AGG CTA CAT GAG ACA GAG TTC ACA-3′	
TGF-β1		TaqMan
Forward	5′-TGC TTC CGC ATC ACC GT-3′	
Reverse	5′-TAG TAG ACG ATG GGC AGT GGC-3′	
Probe	5′-CTG CGT GCC GCA GGC TTT GG-3′	
Collagen IA2		TaqMan
Forward	5′-AAG GGT CCT TCT GGA GAA CC-3′	
Reverse	5′-TCG AGA GCC AGG GAG ACC CA-3′	
Probe	5′-CAG GGT CTT CTT GGT GCT CCC GGT AT-3′	
α-SMA		TaqMan
Forward	5′-GAG GAG CAT CCG ACC TTGC-3′	
Reverse	5′-TTT CTC CCG GTT GGC CTTA-3′	
Probe	5′-AAC GGA GGC GCC GCT GAA CC-3′	
MMP-2		TaqMan
Forward	5′-CCG AGG ACT ATG ACC GGG ATA A-3′	
Reverse	5′-CTT GTT GCC CAG GAA AGT GAA G-3′	
Probe	5′-TCT GCC CCG AGA CCG CTA TGT CCA-3′	
MMP-9		SYBR Green
Forward	5′-GAC AAT CCT TGC AAT GTG GAT G-3′	
Reverse	5′-CCG ACC GTC CTT GAA GAA ATG-3′	
MMP-13		SYBR Green
Forward	5′-TGA CCT GGG ATT TCC AAA AGA G-3′	
Reverse	5′-TCT TCC CCG TGT CCT CAA A-3′	
TIMP-1		SYBR Green
Forward	5′-TCA GCC ATC CCT TGC AAA-3′	
Reverse	5′-GAG CCC ATG AGG ATC TGA TCT-3′	

Table 1 Continued

Primer name	*Sequence*	*Note*
Caspase-12		SYBR Green
Forward	5′-GGC AGA CAT ACT GGT ACT ATT TGG G-3′	
Reverse	5′-GCT CAA CAC ACA TTC CTC ATC TGT-3′	
Caspase-9		SYBR Green
Forward	5′-TGG ACA TTG GTT CTG GCA GAG-3′	
Reverse	5′-GTG TAT GCC ATA TCT GCA TGT CTC-3′	
Caspase-7		SYBR Green
Forward	5′-TAC AAG ATC CCG GTG GAA GCT-3′	
Reverse	5′-CTG GGT TCC TCC ACG AAT AAT AG-3′	
Caspase-3		SYBR Green
Forward	5′-AGA AAT TCA AGG GAC GGG TC-3′	
Reverse	5′-TGC GCG TAC AGT TTC AGC A-3′	
GRP78		SYBR Green
Forward	5′-CCA TCA CCA ATG ACC AAA ACC-3′	
Reverse	5′-GCG CTC TTT GAG CTT TTT GTC T-3′	
ERp57		SYBR Green
Forward	5′-TGAATGCTGAAGACAAGGACGTG-3′	
Reverse	5′-CATTGGCTGTGGCATCCATC-3′	
BAX		SYBR Green
Forward	5′-TAAAGTGCCCGAGCTGATCAGAACC-3′	
Reverse	5′-CCTGGTCTTGGATCCAGACAAGCA-3′	
BAK		SYBR Green
Forward	5′-GAGTTTGCGTAGAGACCCCATCCT-3′	
Reverse	5′-CCACAAATTGGCCCAACAGAACCA-3′	
Bcl-xl		SYBR Green
Forward	5′-TGCGTGGAAAGCGTAGACAAGGA-3′	
Reverse	5′-AAGGCTCTAGGTGGTCATTCAGGT-3′	

Table 1 Continued

Primer name	*Sequence*	*Note*
Bcl-2		SYBR Green
Forward	5′-TCGCGACTTTGCAGAGATGTCC-3′	
Reverse	5′-ACCCCATCCCTGAAGAGTTCCT-3′	
IL-6		
Forward	5′-TGT CTC GAG CCC ACC AGG-3′	TaqMan
Reverse	5′-TGC GGA GAG AAA CTT CAT AGC TG-3′	
Probe	5′-CGA AAG TCA ACT CCA TCT GCC CTT CAG G-3′	
STAT3		
Forward	5′-CAA TAC CAT TGA CCT GCC GAT-3′	SYBR Green
Reverse	5′-CCC CGT TAT TTC CAA ACT GC-3′	
GAPDH		TaqMan
Forward	5′-AAG ATG GTG AAG GTC GGT GTG-3′	
Reverse	5′-GAA GGC AGC CCT GGT AACC-3′	
Probe	5′-CGG ATT TGG CCG TAT CGG ACGC-3′	
GAPDH		SYBR Green
Forward	5′-AAT GCA TCC TGC ACC ACC AAC TGC-3′	
Reverse	5′-GGA GGC CAT GTA GGC CATG AGG TC-3′	

and 98.5 ± 14.9 IU/ml in group M and from 51.2 ± 13.8 and 35.4 ± 3.3 IU/ml in group R, respectively ($P<0.01$). Cells positive for CD68, a marker of activated Kupffer cells, increased in number (Figure 2b) in group M. The expression of TNF-α mRNA, which is known to be derived from activated Kupffer cells in the liver, increased to 2.5-fold in group M (Figure 2e, $P<0.01$) compared with group C, and returned to the normal range in group R ($P<0.01$). These results indicate that the change in diet from MCDD to CD reduced inflammatory reactions, Kupffer cell activation, and AST/ALT release from hepatocytes.

Oxidative Stress and its Recovery in Steatohepatitis

We used the immunostaining of 4-HNE to detect the production of oxidative aldehyde by lipid peroxidation in the liver. As shown in Figure 3a, the control liver of group C exhibited negligible staining by anti-4-HNE antibodies. In contrast, the liver in group M showed brown-colored hepatocytes and stained cells also accumulated at necrotic foci (magnified area). The number of 4-HNE-positive cells and the amount of granulomatous accumulation in cells, presumably macrophages, were clearly reduced in group R.

These results were reproduced on immunostaining of HO-1. As shown in Figure 3b, HO-1 expression is restricted in hepatic sinusoids, presumably in Kupffer cells (magnified area). However, in group M, HO-1-positive cells additionally led to an aggregation of cells next to vacuolized hepatocytes (magnified area). These reactions immediately disappeared in group R. In accordance with these results, HO-1 mRNA expression determined by RT-PCR was significantly augmented in group M compared with group C (5.19 ± 1.08 *vs* 3.13 ± 0.26, respectively, $P<0.01$) and returned to the normal level in group R.

Taken together, it can be stated that the accumulation of Oil red O-stained lipids, 4-HNE, and CD68- and HO-1-positive macrophages by administering an MCDD diet generates oxidative stress and hepatocyte damage (increase in AST and ALT levels), resulting in inflammatory gene expression, such as TNF-α. However, switching the diet from MCDD to CD immediately triggers the inhibition of inflammatory reactions.

Regression of Fibrosis and Hepatic Stellate Cell Activation in Steatohepatitis

Sirius Red staining (Figure 4a) clearly revealed collagen deposition with C-C and P-C bridges, near to cirrhosis, in the fibrotic septum of group M, although collagen deposition was observed only around veins in the intact liver (group C). An immediate and marked recovery of this advanced fibrosis was observed in group R, indicating that the change in diet from MCDD to CD triggers the regression of fibrosis in the liver within 2 weeks.

Immunohistochemistry of α-SMA and cytoglobin, markers of activated stellate cells and liver myofibroblasts, showed that hepatic fibrotic cell activation occurred in group M, whereas the process ceased immediately in group R (Figure 4b and c). Immunoblot analyses confirmed these immunohistochemical observations (Figure 4d). Furthermore, as shown in Figure 4e, RT-PCR analyses indicated that mRNA expressions of all α-SMA, TGF-β1, Col1A2, TIMP-1, MMP-2, and MMP-9 increased significantly in group M, and thereafter returned to the original level in group R. Conversely, the expression of MMP-13 decreased significantly in group M (0.98 ± 0.30 *vs* 3.39 ± 1.24, $P<0.01$) and recovered significantly in group R (2.30 ± 1.11). Thus, the recovery of fibrosis is evident at levels of histology, fibrotic protein, and fibrotic gene expression after switching the diet from MCDD to CD.

The Change of Hepatocyte Apoptosis and Proliferation

TUNEL staining showed that the number of apoptotic hepatocytes slightly increased in group M compared with group C (68.2 ± 15.9 *vs* 40.3 ± 8.33 cells per field, respectively, $P<0.05$), whereas it decreased significantly in group R (48.0 ± 6.48 cells per field) (Figure 5a and c).

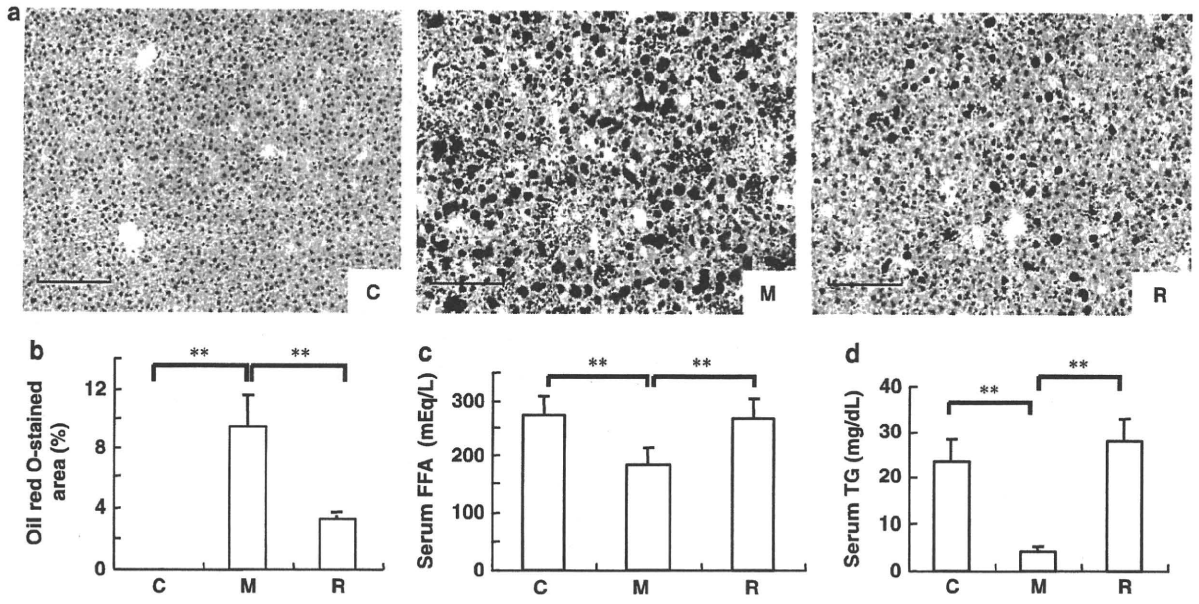

Figure 1 Oil red O staining in the liver and the serum level of FFA and TG. (**a**) Oil red O staining (× 200). Five sections per group were measured. Bar, 25 μm. (**b**) Percentage of Oil red O-stained area was determined using an image analyzer (LuminaVision). Group C, 0%; group M, 9.45% ($P<0.01$ compared with group C); group R, 3.27% ($P<0.01$ compared with group M). (**c**) Serum level of FFA (μequiv./l). $^{**}P<0.01$. (**d**) Serum level of TG (mg/dl). $^{**}P<0.01$.

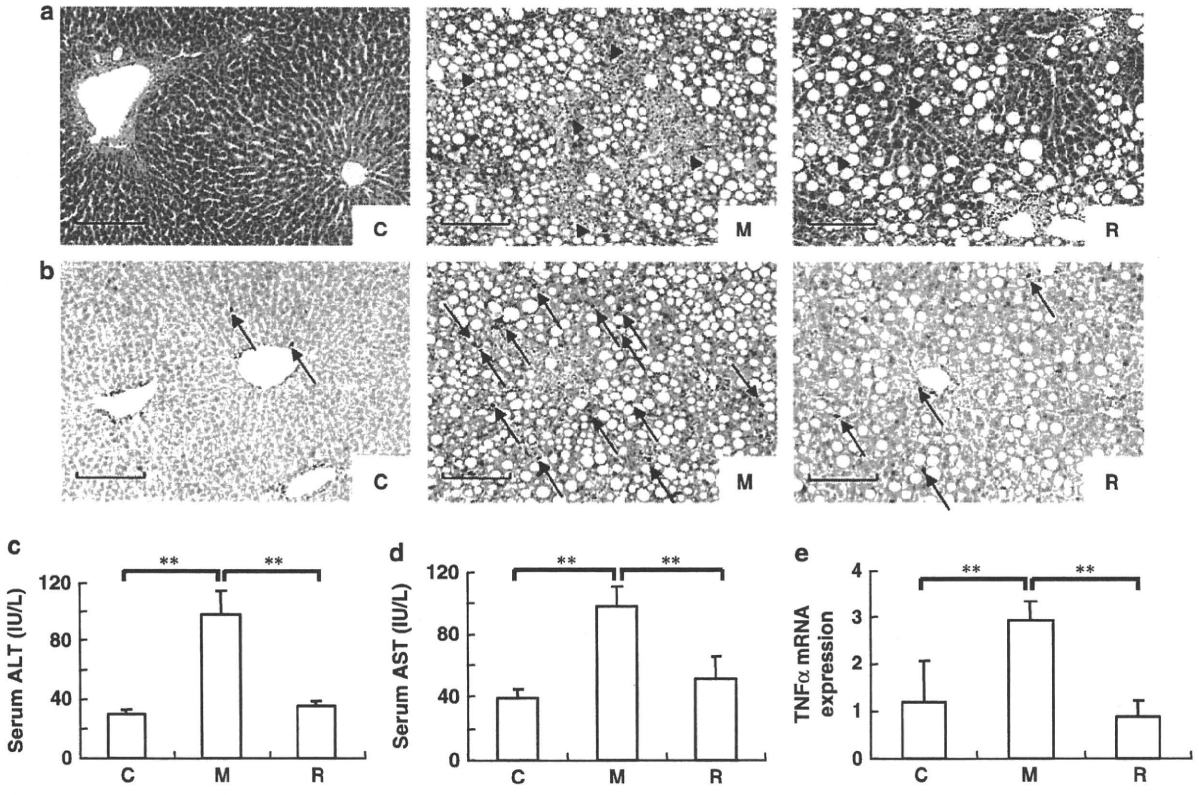

Figure 2 Kupffer cell activation and inflammation. (**a**) H&E staining (× 200). In group M, hepatocytes with fatty degeneration and inflammatory cell foci (arrowheads) were distributed in the parenchyma, whereas their number decreased in group R. Bar, 25 μm. (**b**) CD68 immunostaining (arrows) (× 200). CD68, a macrophage marker and low-density lipoprotein binding site, was rare in group C, whereas CD68-positive cells increased in number in group M, and decreased in group R. Bar, 25 μm. (**c** and **d**) Serum levels of ALT and AST. (**e**) The relative TNF-α mRNA level measured by RT-PCR. The TNF-α mRNA level was normalized by the GAPDH mRNA level.